Article

Mechanism of BRCA1–BARD1 function in DNA end resection and DNA protection

https://doi.org/10.1038/s41586-024-07909-9

Received: 20 November 2023

Accepted: 5 August 2024

Published online: 11 September 2024

Open access

Check for updates

Ilaria Ceppi[1,11], Maria Rosaria Dello Stritto[1,11], Martin Mütze[2], Stefan Braunshier[1], Valentina Mengoli[1], Giordano Reginato[1], Hồ Mỹ Phúc Võ[3,4], Sonia Jimeno[5,6], Ananya Acharya[1], Megha Roy[1], Aurore Sanchez[1,8], Swagata Halder[1,9], Sean Michael Howard[1,10], Raphaël Guérois[7], Pablo Huertas[5,6], Sylvie M. Noordermeer[3,4], Ralf Seidel[2] & Petr Cejka[1]✉

DNA double-strand break (DSB) repair by homologous recombination is initiated by DNA end resection, a process involving the controlled degradation of the 5′-terminated strands at DSB sites[1,2]. The breast cancer suppressor BRCA1–BARD1 not only promotes resection and homologous recombination, but it also protects DNA upon replication stress[1,3–9]. BRCA1–BARD1 counteracts the anti-resection and pro-non-homologous end-joining factor 53BP1, but whether it functions in resection directly has been unclear[10–16]. Using purified recombinant proteins, we show here that BRCA1–BARD1 directly promotes long-range DNA end resection pathways catalysed by the EXO1 or DNA2 nucleases. In the DNA2-dependent pathway, BRCA1–BARD1 stimulates DNA unwinding by the Werner or Bloom helicase. Together with MRE11–RAD50–NBS1 and phosphorylated CtIP, BRCA1–BARD1 forms the BRCA1–C complex[17,18], which stimulates resection synergistically to an even greater extent. A mutation in phosphorylated CtIP (S327A), which disrupts its binding to the BRCT repeats of BRCA1 and hence the integrity of the BRCA1–C complex[19–21], inhibits resection, showing that BRCA1–C is a functionally integrated ensemble. Whereas BRCA1–BARD1 stimulates resection in DSB repair, it paradoxically also protects replication forks from unscheduled degradation upon stress, which involves a homologous recombination-independent function of the recombinase RAD51 (refs. 4–6,8). We show that in the presence of RAD51, BRCA1–BARD1 instead inhibits DNA degradation. On the basis of our data, the presence and local concentration of RAD51 might determine the balance between the pronuclease and the DNA protection functions of BRCA1–BARD1 in various physiological contexts.

DNA end resection includes two mechanistically distinct steps. The initial short-range resection involves a nucleolytic function of the MRE11 nuclease acting within the MRE11–RAD50–NBS1 (MRN) complex, stimulated by phosphorylated CtIP (pCtIP)[1,22,23]. The subsequent long-range resection is carried out by either of two nucleases, EXO1 or DNA2 (refs. 1,22,24). Whereas EXO1 acts on double-stranded DNA (dsDNA), DNA2 nuclease is single-stranded DNA (ssDNA) specific and thus requires a RecQ family helicase partner, Bloom (BLM) or Werner (WRN), together with the ssDNA binding protein replication protein A (RPA)[1,25]. However, a significant crosstalk exists between the resection pathways[24,26–30]. BRCA1–BARD1 promotes resection, as well as the downstream steps in the homologous recombination pathway, including RAD51 loading and strand invasion, probably in complex with BRCA2 (refs. 3,8,9,30). The pro-resection and homologous recombination function of BRCA1 is diminished in cells lacking 53BP1 (refs. 10–12), showing that the primary function of BRCA1–BARD1 in resection is to counteract 53BP1 and its effectors. Whether BRCA1 functions directly to promote resection, or whether its effect is largely indirect has not been clear. BRCA1 binds the MRN complex and CtIP, forming the BRCA1–C complex[17,18,30]. Efficient BRCA1–CtIP interaction is cell-cycle regulated and depends on the CDK-dependent phosphorylation of CtIP at the S327 site[19–21]. Consequently, the non-phosphorylatable CtIP-S327A mutant has resection and recombination defects according to some reports[16,17,31,32], whereas other studies failed to observe a phenotype[10,33,34], suggesting that the contribution of the BRCA1–CtIP interaction to resection may be redundant with other pathways or subject to suppressor mutations. CtIP stimulates DNA end resection by promoting the nuclease of MRN[23], DNA unwinding by BLM[29] and the

[1]Institute for Research in Biomedicine, Università della Svizzera italiana (USI), Faculty of Biomedical Sciences, Bellinzona, Switzerland. [2]Peter Debye Institute for Soft Matter Physics, Universität Leipzig, Leipzig, Germany. [3]Leiden University Medical Center, Leiden, the Netherlands. [4]Oncode Institute, Utrecht, the Netherlands. [5]Departamento de Genética, Facultad de Biología, Universidad de Sevilla, Sevilla, Spain. [6]Centro Andaluz de Biología Molecular y Medicina Regenerativa-CABIMER, Universidad de Sevilla-CSIC-Universidad Pablo de Olavide, Sevilla, Spain. [7]Institute for Integrative Biology of the Cell (I2BC), Commissariat à l'Energie Atomique, CNRS, Université Paris-Sud, Université Paris-Saclay, Gif-sur-Yvette, France. [8]Present address: Institut Curie, Paris Sciences and Lettres University, Sorbonne Université, CNRS UMR 3244, Dynamics of Genetic Information, Paris, France. [9]Present address: Biological Systems Engineering, Plaksha University, Mohali, India. [10]Present address: Department of Mechanical and Biomedical Engineering, Boise State University, Boise, ID, USA. [11]These authors contributed equally: Ilaria Ceppi, Maria Rosaria Dello Stritto. ✉e-mail: petr.cejka@irb.usi.ch

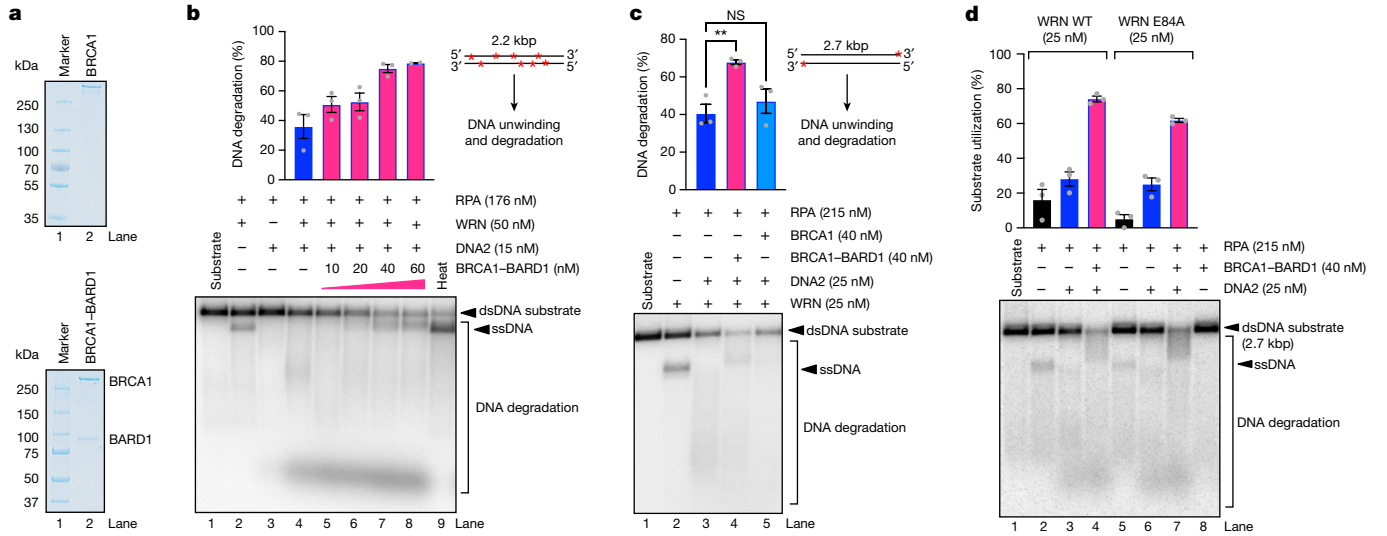

Fig. 1 | BRCA1–BARD1 directly promotes resection by WRN-DNA2-RPA. **a**, Recombinant BRCA1 (top) and the BRCA1–BARD1 (bottom) complex used in this study. The polyacrylamide gels were stained with Coomassie Brilliant Blue. **b**, Resection assays with WRN-DNA2-RPA, and its stimulation by BRCA1–BARD1. Top right, a schematic of the assay. Red asterisks (*) represent the position of the radioactive labels. Top, quantitation of DNA degradation. Averages shown; error bars, s.e.m. (lanes 4–7); $n = 2$ for the reaction containing 60 nM of BRCA1–BARD1 and $n = 3$ for all the other samples. Bottom, representative assays. **c**, Resection assays with WRN-DNA2-RPA, in the absence or presence of either BRCA1–BARD1 or BRCA1. Top right, a schematic of the assay. Red asterisks (*) represent the position of the radioactive labels. Top, quantitation of DNA degradation. Averages shown; error bars, s.e.m.; $n = 3$. $^{**}P = 0.0055$, two-tailed *t*-test. Bottom, representative assays. **d**, Resection assays with DNA2-RPA, and either wild-type (WT) WRN or exonuclease-dead WRN E84A, in the absence or presence of BRCA1–BARD1. Top, quantitation of the substrate utilization. Averages shown; error bars, s.e.m.; $n = 3$. Bottom, representative assays. Source data are provided in Supplementary Fig. 1. NS, not significant.

helicase-nuclease DNA2 (refs. 27,28). Whether any of these reactions is directly regulated by the BRCA1–BARD1 complex was not known.

BRCA1–BARD1 stimulates DNA end resection

To identify a potential direct function of BRCA1–BARD1 in DSB processing, we reconstituted DNA end resection reactions in vitro with purified recombinant proteins. BRCA1 was expressed in insect *Spodoptera frugiperda* 9 (*Sf*9) cells either on its own, or as a heterocomplex with BARD1, with approximate 1:1 stoichiometry (Fig. 1a). BRCA1, as well as BRCA1–BARD1, were largely mono- or heterodimeric (Extended Data Fig. 1a). BRCA1 was tagged with 2× maltose-binding protein (MBP) tag at the N terminus, which improved yield and solubility. We did not observe any effect of BRCA1–BARD1 on the endonuclease activity of MRN in conjunction with pCtIP, nor on the exonuclease activity of MRE11–RAD50, which function in the initial short-range resection (Extended Data Fig. 1b–d). However, BRCA1–BARD1 notably promoted long-range resection catalysed by WRN and DNA2 together with RPA (Fig. 1b and Extended Data Fig. 1b,e). The long-range resection by WRN-DNA2-RPA is dependent on DNA unwinding by WRN, which is thought to occur in a concerted manner with 5′–3′ ssDNA degradation by DNA2 (ref. 35). Both DNA unwinding and degradation are stimulated by RPA, which establishes the correct polarity of DNA end resection[1]. The accumulation of a partially resected DNA intermediate in Fig. 1b (lanes 7 and 8) suggested that BRCA1–BARD1 may promote DNA unwinding by WRN, resulting in accelerated DNA unwinding that was partially uncoupled from DNA degradation by DNA2. In accord, the intermediate was not visible at lower WRN concentrations, while the stimulatory effect of BRCA1–BARD1 remained apparent (Extended Data Fig. 1f). We note that the MBP tag on BRCA1 did not interfere with the stimulatory capacity of BRCA1–BARD1 on WRN-DNA2-RPA (Extended Data Fig. 1g,h). BRCA1 alone (without BARD1) did not significantly stimulate DNA end resection by WRN-DNA2-RPA, showing that the BRCA1–BARD1 heterodimer is necessary (Fig. 1c). Resection did not require the exonuclease activity of WRN (Fig. 1d and Extended Data Fig. 1i), whereas it was dependent on the WRN helicase activity and ATP hydrolysis (Extended Data Fig. 1i,j). The DNA degradation activity was entirely dependent on the nuclease active site of DNA2 (Extended Data Fig. 1i,j). BRCA1–BARD1 did not show any activity per se, showing that it is an accessory factor (Extended Data Fig. 1h,j). Together, we establish that the BRCA1–BARD1 heterodimer directly stimulates long-range DNA end resection by WRN-DNA2-RPA.

BRCA1–BARD1 promotes WRN helicase

To define how the BRCA1–BARD1 complex promotes DNA end resection by WRN-DNA2-RPA, we divided the resection reaction into its components. We observed that BRCA1–BARD1 promoted DNA unwinding by WRN-RPA on both short oligonucleotide-based and long dsDNA substrates, but not by nuclease-dead yeast Dna2 E675A (*Sc*Dna2 E675A) used as a non-cognate negative control[36] (Extended Data Fig. 2a–d). BRCA1–BARD1 also stimulated WRN ATPase activity (Extended Data Fig. 2e). To obtain more quantitative data, we turned to single-molecule magnetic tweezers. In our setup, 6.1 kilobase pair (kbp) long dsDNA with a 5′ ssDNA flap was on one side attached to a fixed surface, and on the other side to a mobile magnetic bead[37] (Fig. 2a). Owing to the length difference between ssDNA and dsDNA, DNA unwinding can be inferred from the relative bead position. BRCA1–BARD1 moderately stimulated both the processivity (160 versus 283 bp) and the rate (26 versus 34 bp per second) of DNA unwinding by WRN-RPA (Fig. 2b–g and Extended Data Fig. 2f,g). Moreover, with WRN-RPA alone, we observed both DNA unwinding and rewinding events (Fig. 2b,h and Extended Data Fig. 2f), probably resulting from frequent DNA strand switching by WRN, reminiscent of yeast Sgs1 (ref. 37). In the presence of BRCA1–BARD1, the rewinding events were strongly reduced (Fig. 2c,h and Extended Data Fig. 2g), which notably enhanced the extent of DNA being unwound (Fig. 2b,c). BRCA1–BARD1 and/or RPA showed no activity per se in the tweezer experiments (Extended Data Fig. 2h). In contrast to a strong direct effect on WRN, BRCA1–BARD1 did not notably stimulate the nuclease activity of DNA2-RPA, when

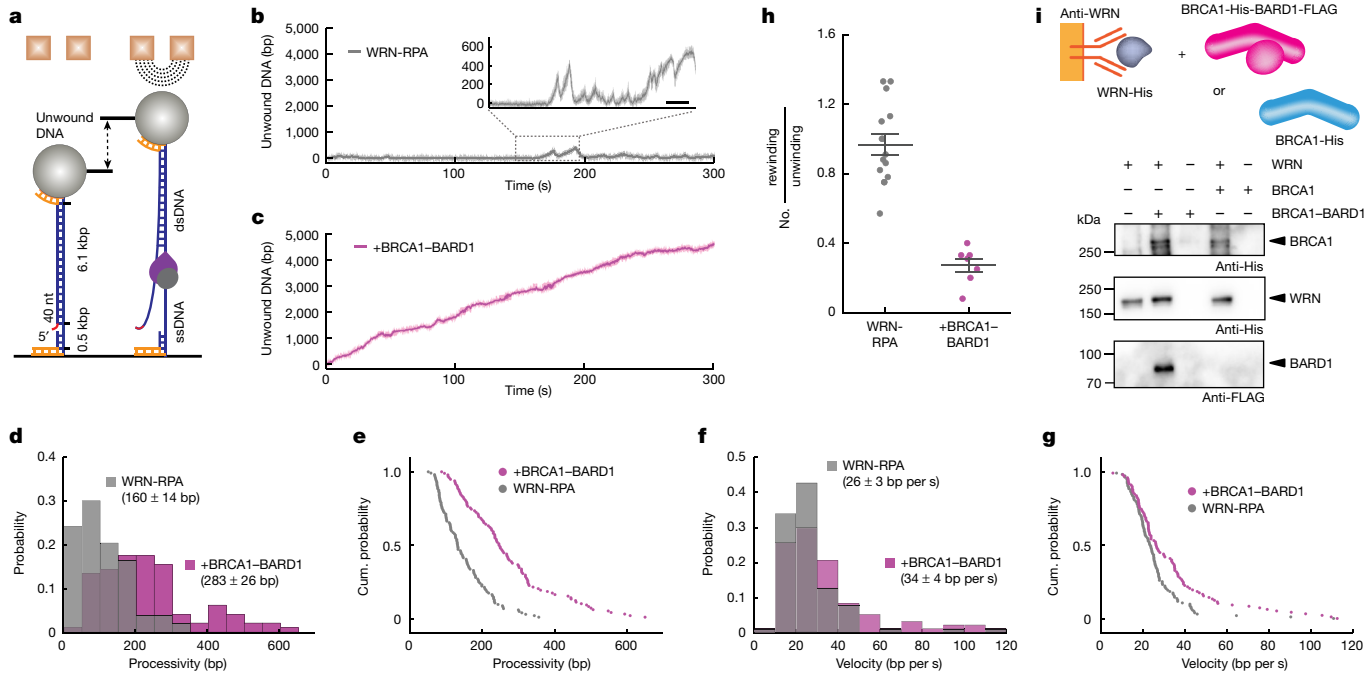

Fig. 2 | BRCA1–BARD1 promotes WRN-mediated DNA unwinding. **a**, A schematic of the single-molecule magnetic tweezers assay setup used and the DNA substrate. **b**, Representative trajectory of DNA unwinding events by WRN in the presence of RPA, both 25 nM. A zoomed-in view highlighting unwinding and rewinding events is shown in the dashed square. Scale bar, 10 s. **c**, Representative trajectory of DNA unwinding events by WRN (25 nM) in the presence of BRCA1–BARD1 (40 nM) and RPA (25 nM). **d**,**e**, Processivity histogram (**d**) and cumulative (Cum.) probability distribution (shown as survival probability) (**e**) of the observed DNA unwinding events by WRN-RPA, both 25 nM, in the absence (grey) or presence (pink) of BRCA1–BARD1 (40 nM), with mean values of 160 ± 14 bp (n = 104) and 283 ± 26 bp (n = 98), respectively. Error, 2 s.e.m. **f**,**g**, Velocity histogram (**f**) and cumulative probability distribution (shown as survival probability) (**g**) of the observed DNA unwinding events by WRN-RPA, both 25 nM, in the absence (grey) or presence (pink) of BRCA1–BARD1 (40 nM), with mean values of 26 ± 3 bp per second (n = 104) and 34 ± 4 bp per second (n = 98), respectively. Error, 2 s.e.m. **h**, Ratio of rewinding (DNA shortening) and unwinding (DNA extension) events by WRN-RPA, both 25 nM, in the absence (grey) or presence (pink) of BRCA1–BARD1 (40 nM). Averages shown; error bars, s.e.m.; n = 15 (in the absence of BRCA1–BARD1) and n = 7 (in the presence of BRCA1–BARD1). **i**, Representative protein-interaction assays. Top, a schematic of the assay. Source data are provided in Supplementary Fig. 1. nt, nucleotides; s, second.

ssDNA was used as a substrate (Extended Data Fig. 2i). DNA2, in addition to its essential nuclease function, has an ATPase-driven motor activity that acts as a ssDNA translocase in DNA end resection[1,27,28,38,39]. BRCA1–BARD1 did not efficiently stimulate the ATPase activity of wild-type DNA2 or nuclease-dead DNA2 D277A (Extended Data Fig. 2j). The stimulatory effect of BRCA1–BARD1 on the WRN helicase is underpinned by a direct physical interaction as observed in in vitro pull-down assays, which also showed that BARD1 is dispensable for the physical interaction with WRN (Fig. 2i), in agreement with experiments performed using cell extracts[36]. Together, we conclude that BRCA1–BARD1 stimulates the DNA2 nuclease-dependent branch of long-range DNA end resection by promoting the WRN helicase activity. Our single-molecule experiments determined that BRCA1–BARD1 supports WRN during the course of DNA unwinding, and it is not simply a recruitment factor[40].

BRCA1–BARD1 functions with CtIP

MRN and pCtIP together with BRCA1–BARD1 form the cell-cycle stage-dependent BRCA1–C complex that has been broadly implicated in DNA resection and homologous recombination[17,18,30], but the mechanism of its function remained unclear. It has been previously established that MRN and pCtIP, components of the short-range resection, have extra structural, nuclease-independent functions to stimulate long-range resection[24,26–29]. In this context, both MRN and pCtIP were shown to facilitate the recruitment and activity of BLM[24,29], but their interplay with WRN was not known. pCtIP also promotes the motor function of DNA2, which in turn enhances the rate of DNA degradation by the nuclease activity of DNA2 (refs. 28,40). We next set out to test for the effect of BRCA1–BARD1 on the WRN-DNA2-RPA-dependent resection when MRN and/or pCtIP were present. With pCtIP, the stimulation of WRN-DNA2-RPA by BRCA1–BARD1 was even more apparent (Extended Data Fig. 2k,l, compare with Extended Data Fig. 1e). These data agree with our previous observations that pCtIP promotes ssDNA degradation by DNA2 through the stimulation of its motor activity[28,41], and hence DNA2-CtIP can keep up with accelerated DNA unwinding by WRN-BRCA1–BARD1.

We next used λDNA/HindIII digest as a substrate to monitor DNA degradation of dsDNA fragments of various lengths up to 23 kbp (Extended Data Fig. 2m). In the absence of pCtIP (Fig. 3a, lanes 1–12 and Extended Data Fig. 2n), the stimulation by BRCA1–BARD1 was limited and restricted to the shorter dsDNA fragments. By contrast, with pCtIP, the stimulatory effect of BRCA1–BARD1 was notable, and very efficient degradation of long dsDNA substrates was observed (Fig. 3a, lanes 13–24 and Extended Data Fig. 2n). The DNA end resection activity of the BRCA1–BARD1-pCtIP-WRN-DNA2-RPA ensemble depends on the helicase activity of WRN, the nuclease activity of DNA2 and ATP (Extended Data Fig. 2o). Replacement of wild-type DNA2 with the helicase-dead DNA2 K654R variant within the ensemble also resulted in reduced resection (Extended Data Fig. 2o).

The BLM helicase functions in the DNA2 end resection pathway redundantly with WRN, depending on cell type and biological context[1]. We observed that BRCA1–BARD1 also promoted DNA unwinding by BLM (Fig. 3b, compare lanes 2 and 3), and BRCA1–BARD1 and pCtIP synergistically stimulated resection by BLM-DNA2-RPA (Fig. 3b). By contrast, BRCA1–BARD1 only moderately enhanced the nuclease

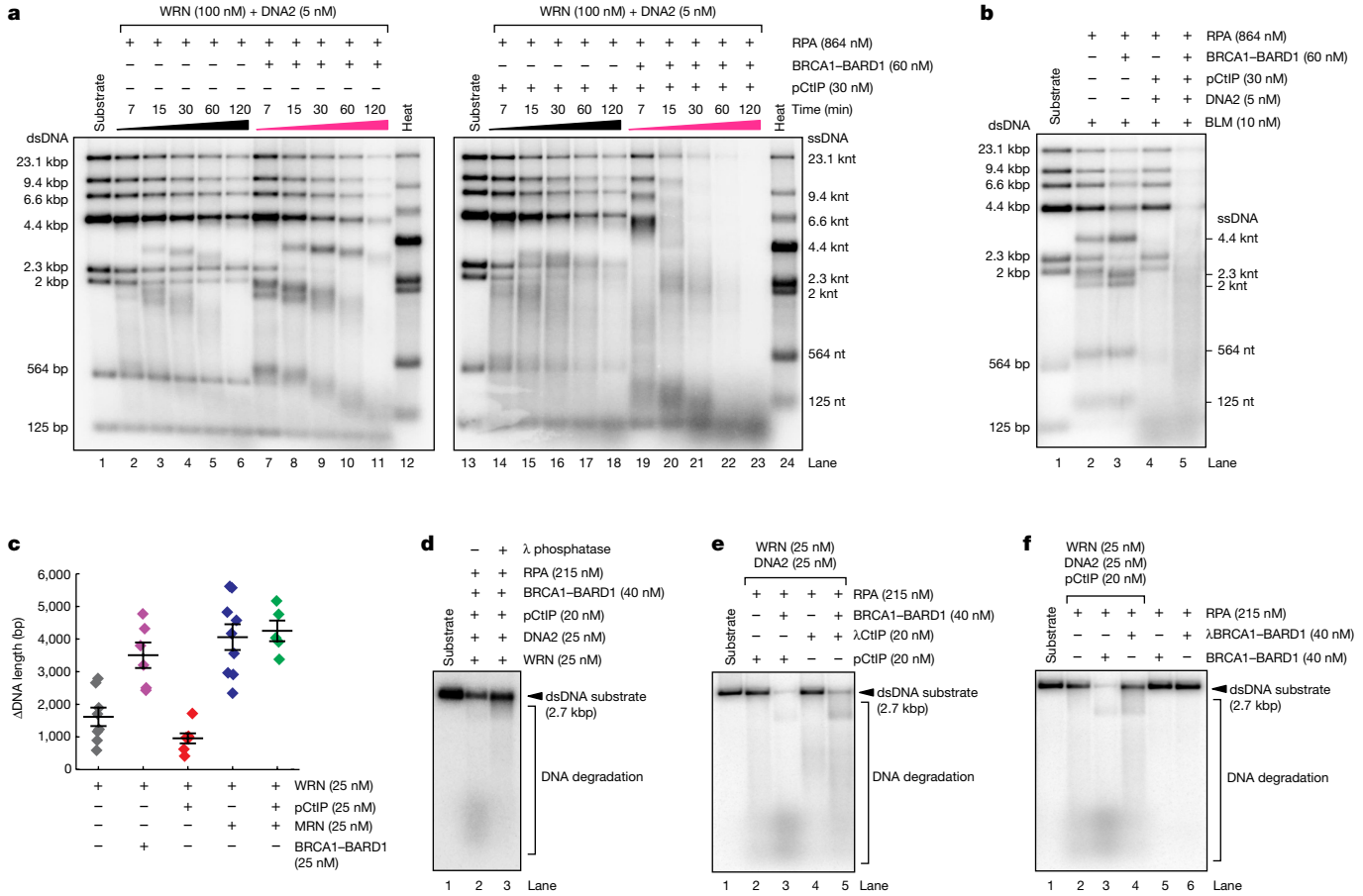

Fig. 3 | BRCA1–BARD1 together with CtIP and MRN promote resection by WRN-DNA2-RPA. a, Representative kinetic resection assays with WRN-DNA2-RPA, in the absence or presence of pCtIP and BRCA1–BARD1. **b**, Representative resection assays with BLM-DNA2-pCtIP-RPA, in the absence or presence of BRCA1–BARD1. **c**, DNA unwinding by the indicated proteins, at 25 nM, expressed as ΔDNA-length (Methods). Averages shown; error bars, s.e.m.; $n = 7$ (for WRN), $n = 6$ (for WRN-BRCA1–BARD1), $n = 7$ (for WRN-BRCA1–BARD1-pCtIP), $n = 9$ (for WRN-MRN-BRCA1–BARD1), $n = 5$ (for WRN-pCtIP-MRN). **d**, Representative resection assays with WRN-DNA2-pCtIP-BRCA1–BARD1-RPA, in the absence or presence of λ phosphatase (200 U). **e**, Representative resection assays with WRN-DNA2-RPA, in the presence of pCtIP or dephosphorylated CtIP (λCtIP) and in the absence or presence of BRCA1–BARD1. **f**, Representative resection assays with WRN-DNA2-pCtIP-RPA, in the absence or presence of either BRCA1–BARD1 (BRCA1–BARD1) or dephosphorylated BRCA1–BARD1 (λBRCA1–BARD1). Source data are provided in Supplementary Fig. 2. knt, kilonucleotides.

activity of DNA2 on ssDNA when pCtIP was also present and BLM and WRN were omitted (Extended Data Fig. 3a). BRCA1–BARD1 did not stimulate the processivity (264 versus 271 bp) nor the rate (57 versus 46 bp per s) of DNA unwinding by nuclease-dead DNA2 D277A in conjunction with RPA and pCtIP (Extended Data Fig. 3b–f).

When MRN was included in the ensemble reaction, resection was even more enhanced (Extended Data Fig. 3g). We observed that MRN promoted dsDNA unwinding by WRN in both ensemble (Extended Data Fig. 3h,i) and single-molecule experiments (Fig. 3c and Extended Data Fig. 3j). pCtIP, instead, had no effect on DNA unwinding by WRN (Fig. 3c and Extended Data Fig. 3j). Our data collectively demonstrate that BRCA1–BARD1, MRN and pCtIP stimulate long-range DNA end resection by WRN/BLM-DNA2-RPA. BRCA1–BARD1 and MRN primarily promote DNA unwinding by WRN/BLM and pCtIP activates DNA2.

Phosphorylation of BRCA1–C complex

We demonstrated that the BRCA1–C complex consisting of BRCA1–BARD1, pCtIP and MRN promotes DNA end resection by WRN-DNA2-RPA. The assembly of the BRCA1–C complex is cell-cycle regulated and it is dependent on protein phosphorylation[17,18,30]. We have observed a strong inhibition of DNA resection when the BRCA1–BARD1-pCtIP-WRN-DNA2-RPA reaction was supplemented with λ phosphatase (Fig. 3d). To determine which of the protein components need to be phosphorylated, we prepared separately BRCA1–BARD1, WRN and CtIP in the presence of λ phosphatase, which was then removed from the final protein pool (Extended Data Fig. 3k). We observed that phosphorylation of both CtIP and BRCA1–BARD1 was important (Fig. 3e,f), whereas λ phosphatase treatment did not affect the function of WRN (Extended Data Fig. 3l).

The binding of phosphorylated S327 of pCtIP by the C-terminal (BRCT) domains of BRCA1 is required for the assembly of the BRCA1–C complex[19–21]. To test whether the physical interaction between pCtIP and BRCA1–BARD1 within the BRCA1–C complex is required for the maximal stimulatory effect, we used the pCtIP S327A mutant known to be impaired in its interaction with BRCA1[19–21] (Fig. 4a,b and Extended Data Fig. 4a). As above, BRCA1–BARD1 strongly stimulated DNA end resection by WRN-DNA2-RPA in the presence of wild-type pCtIP, with or without MRN (Fig. 4b). When wild-type pCtIP was replaced with pCtIP S327A, that is, a variant with non-phosphorylatable S327, but otherwise prepared in the same way as the wild-type phosphorylated protein, BRCA1–BARD1 could not stimulate the reaction (Fig. 4a,b and Extended Data Fig. 4a).

In addition to pCtIP S327 mediating the interaction with BRCA1, the other CtIP region required for its function in the resection ensemble

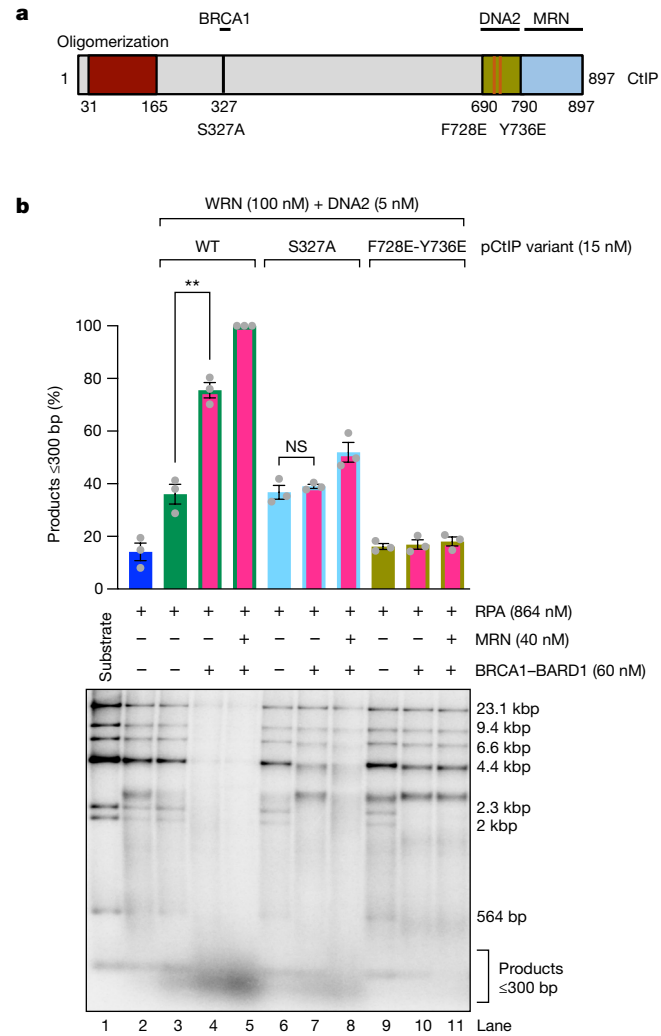

Fig. 4 | The integrity of the BRCA1–C complex is required to promote resection. a, Cartoon of the primary structure of the CtIP protein. Point mutants used in this study are highlighted. **b**, Resection assays with WRN-DNA2-RPA, in the absence or presence of the indicated pCtIP variant, MRN and BRCA1–BARD1. Top, quantitation of DNA degradation (based on the proportion of degradation products of ≤300 bp in length). Averages shown; error bars, s.e.m.; $n = 3$. $^{**}P = 0.0012$, two-tailed t-test. Bottom, representative assays. Source data are provided in Supplementary Fig. 3.

spans residues 690 and 740, including the F728 and Y736 residues (Fig. 4a,b and Extended Data Fig. 4a–c), required for interaction and stimulation of DNA2 (refs. 27,28). By contrast, the C-terminal domain of CtIP, which physically and functionally interacts with MRN in short-range resection[23], was largely dispensable (Extended Data Fig. 4a–c). Nevertheless, MRN further stimulated resection by the ensemble, with both wild-type as well as pCtIP S327A variants (Fig. 4b).

The pCtIP S327A mutant, although supporting DNA resection by WRN-DNA2-RPA in conjunction with BRCA1–BARD1 less efficiently compared to wild-type pCtIP (Fig. 4b), was in contrast not affected in its capacity to promote the nuclease activity of DNA2-RPA on ssDNA (without WRN and BRCA1–BARD1) (Extended Data Fig. 4d), nor in its ability to promote the endonuclease of MRN (Extended Data Fig. 4e). The pCtIP S327A mutant thus specifically disrupts the pCtIP function within the BRCA1–C complex in long-range resection[16]. The assembly of a functional pCtIP and BRCA1–BARD1 complex is therefore necessary for the maximal stimulatory effect in DNA end resection. As BRCA1–BARD1 promotes DNA unwinding by WRN, and pCtIP stimulates DNA degradation by DNA2, the data suggest that DNA unwinding and DNA degradation occur in a concerted manner.

Minimal BRCA1, BARD1 and WRN domains

The primary sequence of BRCA1 includes an N-terminal RING domain necessary for the interaction with BARD1, and C-terminal BRCT repeats that bind pCtIP[8] (Extended Data Fig. 5a). Consequently, the BRCA1(ΔRING)–BARD1 variant did not promote resection (Extended Data Figs. 4a and 5a,b), whereas BRCA1(ΔBRCT)–BARD1, which interacted with BARD1 (Extended Data Fig. 4a), was strongly impaired (Extended Data Fig. 5a,b), as expected. The coiled-coil region of BRCA1 is necessary for the interaction with PALB2-BRCA2, but dispensable for resection[8]. The central BRCA1 region encoded by exon 11 is largely unstructured, mediates many protein–protein interactions and is necessary for resection based on cellular assays[8,42]. To define a potential direct function of the central BRCA1 region in resection, we created a series of internal deletion mutants, which were copurified with BARD1 (Extended Data Figs. 4a and 5a). The BRCA1Δ1–BARD1 variant was impaired, whereas BRCA1Δ2–BARD1 (as well as BRCA1Δ3–BARD1 and BRCA1Δ4–BARD1) could promote resection of the ensemble almost as efficiently as wild-type BRCA1–BARD1 (Extended Data Figs. 4a and 5c,d). The BRCA1 region spanning residues 931 to 1171 is thus necessary for the stimulatory function of the resection ensemble. We found that BRCA1Δ2–BARD1, unlike BRCA1Δ1–BARD1, could promote DNA unwinding by WRN together with RPA (Extended Data Fig. 5e), showing that the identified BRCA1 region disrupts the interplay with WRN. The BRCA1 region between residues 931 and 1171 contains several conserved patches (Extended Data Fig. 5f), including phosphorylation sites necessary for resection but dispensable for BRCA1–C complex assembly[43]. We focused on two of these patches, creating BRCA1(V1035D-F1036D) and BRCA1(Y1127D-I1129D) substitutions within the full-length BRCA1–BARD1 heterodimer (Extended Data Figs. 4a and 5a). We noted that both variants were partially impaired in resection, particularly the BRCA1(V1035D-F1036D)–BARD1 mutant (Extended Data Fig. 5g).

BARD1 similarly contains the N-terminal RING domain mediating its interaction with BRCA1. This domain is followed by a largely unstructured region that was found to bind RAD51, followed by ankyrin repeats (ANK) and the BRCT domain, which mediate interactions with nucleosomes on nascent DNA (H4K20 mark) and poly(ADP-ribose), respectively[8] (Extended Data Fig. 6a). We could not purify BARD1 on its own, but we could prepare several BRCA1–BARD1 variants truncated at the C terminus of BARD1 (Extended Data Fig. 6a,b). Using more restrictive conditions that make resection entirely dependent on BARD1 (Extended Data Fig. 6c,d), we observed that the C-terminal two-thirds of BARD1 (beyond residue 261, including ankyrin and/or BRCT domains) was partially dispensable for resection (Extended Data Fig. 6e). Further truncation eliminating the BARD1 unstructured region completely abrogated resection (Extended Data Fig. 6e), but did not disrupt complex formation with BRCA1 (Extended Data Fig. 6b). Subsequently, we observed that internal deletion of the 123–261 region of BARD1 also entirely disrupted resection (Extended Data Fig. 6f,g). The BARD1 region between residues 123 and 261 contains four conserved patches (Extended Data Fig. 6f), the first of which interacts with SLX4 (MUSIC motif)[44]. We focused on the three subsequent ones (Extended Data Fig. 6a,b,f), and found that particularly the Y180E-F182E mutations in patch 2 (residues 175–190) and the deletion of patch 3 (BRCA1–BARD1Δ205–220) were disruptive for resection (Extended Data Fig. 6a,b,g).

The WRN protein contains an exonuclease domain, followed by a helicase domain, as well as RQC and HRDC domains, typical for members of the RecQ helicase family (Extended Data Fig. 6h,i). We have prepared six WRN truncation variants, and subjected them to DNA end resection assays together with DNA2, RPA and pCtIP, without or with

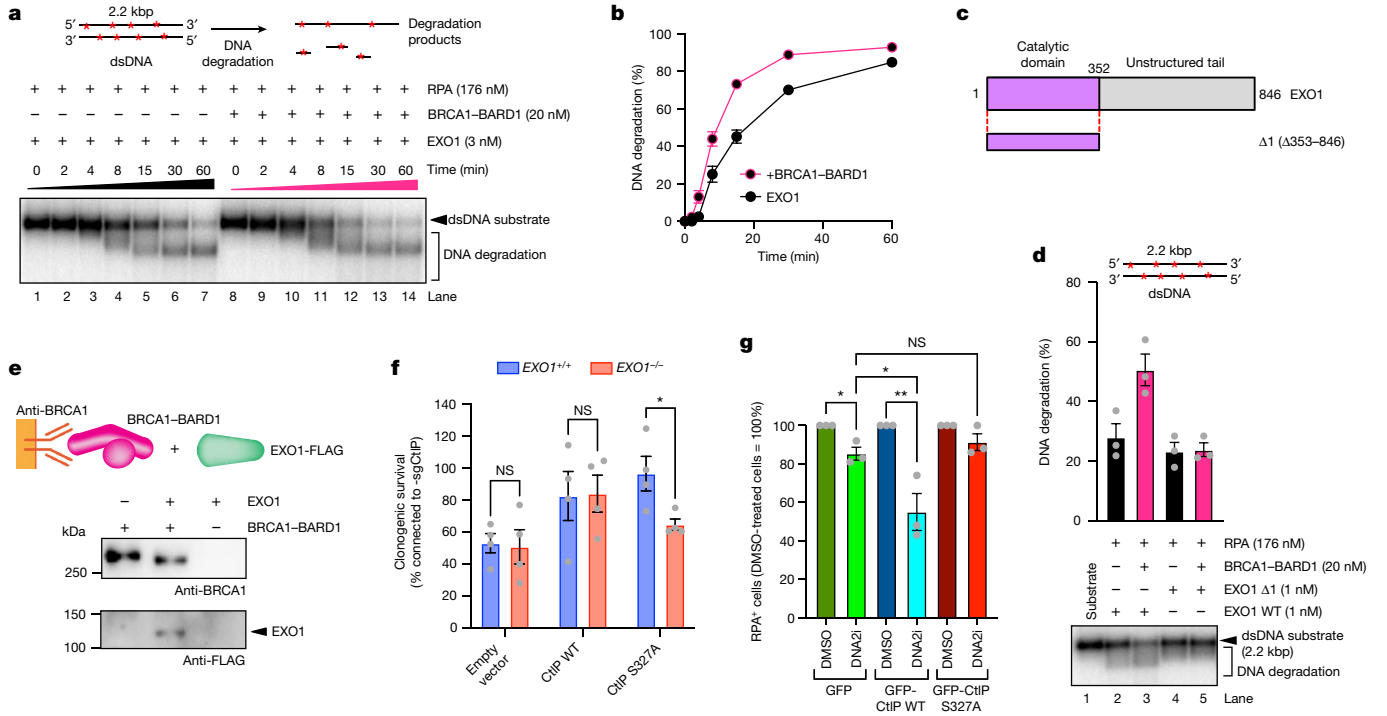

Fig. 5 | BRCA1–BARD1 promotes resection by EXO1 independently of CtIP. **a**, Representative kinetic resection assays with EXO1, RPA, in the absence or presence of BRCA1–BARD1. Top, a schematic of the assay. Red asterisks (*) represent the position of the radioactive labels. **b**, Quantitation of DNA degradation from assays such as shown in **a**. Averages shown; error bars, s.e.m.; $n = 3$. **c**, Cartoon of the primary structure of the EXO1 protein and the Δ1 variant used in the study. **d**, Resection assays with RPA, wild-type EXO1 or EXO1 Δ1, in the absence or presence of BRCA1–BARD1. Top, quantitation of DNA degradation. Averages shown; error bars, s.e.m.; $n = 3$. Bottom, representative assays. **e**, Representative protein-interaction assays. Top, a schematic of the assay. **f**, Quantitation of clonogenic cell survival of RPE1 cells *EXO1*$^{+/+}$ or *EXO1*$^{-/-}$ cells, which were lentivirally transduced with wild-type or S327A CtIP variants, and in which the endogenous CtIP was disrupted by Cas9–gRNA. Averages shown; error bars, s.e.m.; $n = 4$. *$P = 0.0274$, two-tailed *t*-test. **g**, Quantitation of RPA$^+$ cells from an experiment such as shown in Extended Data Fig. 8k. Values were normalized against the DMSO-treated cells. Averages shown; error bars, s.d.; $n = 3$. DMSO- versus DNA2i-treated GFP cells *$P = 0.012$, DMSO- versus DNA2i-treated GFP-CtIP-WT cells **$P = 0.0094$, DNA2i-treated GFP cells versus cells DNA2i-treated GFP-CtIP-WT *$P = 0.041$, two-tailed *t*-test. In all cases, at least 150 cells were studied per condition. Source data are provided in Supplementary Fig. 3.

BRCA1–BARD1 (Extended Data Fig. 6j,k). We observed that BRCA1–BARD1 stimulated resection in conjunction with all tested WRN variants, although to very different extents (Extended Data Fig. 6j,k). Similar data were obtained also without pCtIP (Extended Data Fig. 7a). The resection activity was not affected by the inactivation of the WRN exonuclease domain activity (Extended Data Fig. 7b,c). Single-molecule experiments revealed that the ability to promote resection largely corresponded to the DNA unwinding capacity of the respective WRN variants (Extended Data Fig. 7d,e). Nevertheless, BRCA1–BARD1 promoted DNA unwinding by even the WRN helicase core domain (Extended Data Fig. 7d,e). In accord, BRCA1, independently of BARD1, physically interacted with the WRN helicase core domain, and the interaction was enhanced when further WRN domains were included[36] (Extended Data Fig. 7f). We conclude that the BRCA1 subunit of BRCA1–BARD1 interacts with WRN through many contact points to promote its DNA unwinding activity, which is functionally coupled with DNA degradation by CtIP-DNA2 (Extended Data Fig. 7g).

BRCA1–BARD1 promotes EXO1

The 5′–3′ dsDNA specific EXO1 nuclease represents a second branch of eukaryotic DNA end resection, which functions with the DNA2 pathway in a redundant manner, depending on cellular background and biological context[1]. We observed a moderate stimulation of EXO1 by BRCA1–BARD1 (Fig. 5a,b and Extended Data Fig. 8a). As with the DNA2-dependent branch, the optimal stimulation was observed with the BRCA1–BARD1 heterodimer (as opposed to BRCA1 alone) (Extended Data Fig. 8b). Moreover, BRCA1Δ1–BARD1 was deficient, whereas BRCA1Δ2–BARD1 was proficient in EXO1 stimulation (Extended Data Fig. 8c). However, in contrast to the reactions with DNA2, pCtIP did not stimulate the EXO1 branch even in the presence of BRCA1–BARD1 (ref. 27) (Extended Data Fig. 8d–f). EXO1 contains an N-terminal structured nuclease core domain, followed by largely unstructured C-terminal tail (Fig. 5c). Truncated EXO1Δ1 (Δ353–846) shows a similar nuclease activity as full-length EXO1 (Extended Data Fig. 8g), but it fails to be stimulated by BRCA1–BARD1 (Fig. 5d). Hence, the C-terminal region of EXO1 contains residues that are necessary for the interplay with BRCA1–BARD1. Furthermore, we note that BRCA1–BARD1 instead moderately inhibited the *Escherichia coli* ExoIII nuclease used as a non-cognate negative control (Extended Data Fig. 8h), probably due to competition for DNA access, establishing thus a specificity for the BRCA1–BARD1 and human EXO1 interplay (Extended Data Fig. 8h,i). Accordingly, we found that BRCA1–BARD1 directly physically interacts with EXO1 (Fig. 5e).

CtIP–BRCA1 largely promotes DNA2 pathway

Recently, BRCA1 and EXO1 were found to show synthetic lethality[45,46]. Because our experiments suggested that CtIP promotes the DNA2-dependent pathway and not the EXO1 pathway, we proposed that the CtIP-S327A mutation might be more toxic in the EXO1-deficient background. To this point, we used RPE1 *EXO1*$^{+/+}$ or *EXO1*$^{-/-}$ cells, which were lentivirally transduced with wild-type or S327A CtIP variants, and in which the endogenous CtIP was disrupted by Cas9–gRNA (Extended

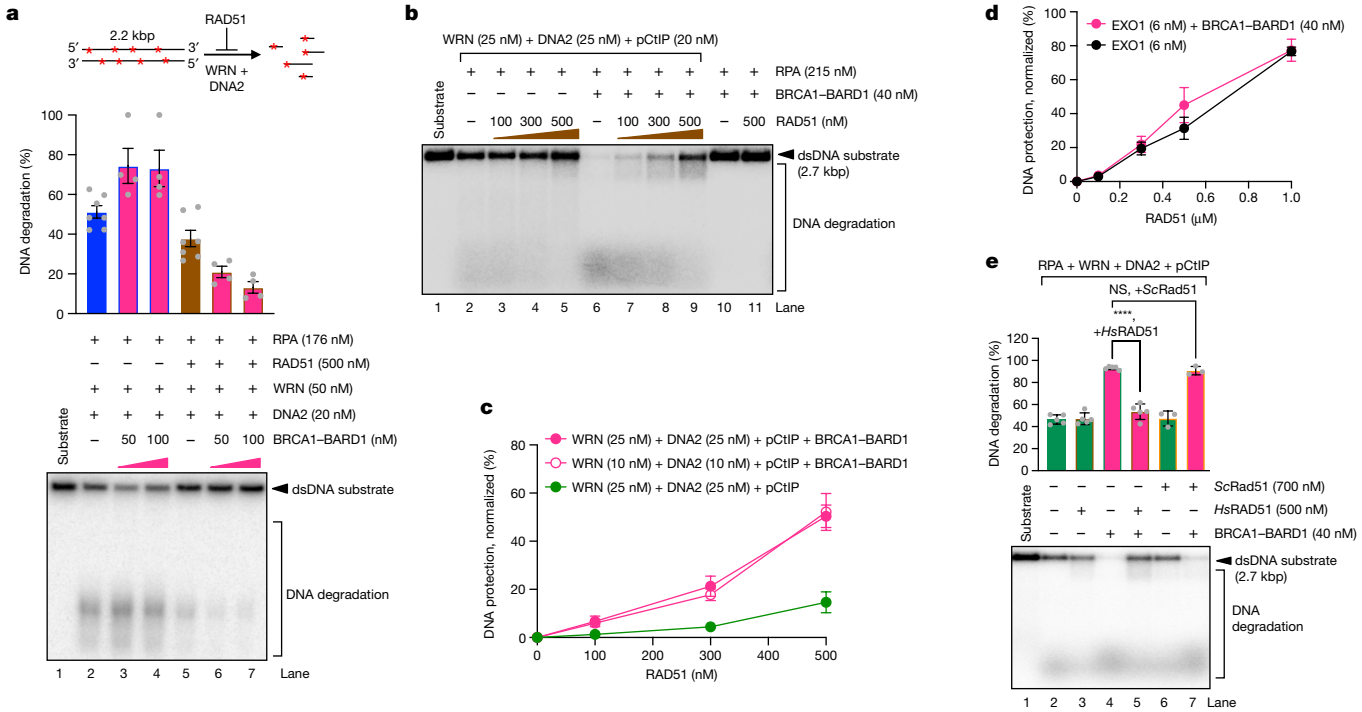

Fig. 6 | BRCA1–BARD1 enhances RAD51-mediated DNA protection. **a**, DNA protection assays with WRN-DNA2-RPA, in the absence or presence of BRCA1–BARD1 and RAD51, performed at 100 mM NaCl. Top, a schematic of the assay. Red asterisks (*) represent the position of the radioactive labels. Middle, quantitation of DNA degradation. Averages shown; error bars, s.e.m.; $n = 7$ (in the absence of BRCA1–BARD1) and $n = 4$ (in the presence of BRCA1–BARD1). Bottom, representative assays. **b**, Representative protection assays with WRN-DNA2-pCtIP-RPA, in the absence or presence of BRCA1–BARD1 and increasing concentration of RAD51. **c**, Quantitation of DNA protection assays such as shown in **b**. Averages shown; error bars, s.e.m.; $n = 4$. The data were normalized to the corresponding reaction without RAD51 (lane 2). Values without normalization are plotted in Extended Data Fig. 9g. Representative protection assays with WRN (10 nM) and DNA2 (10 nM), in presence of pCtIP and BRCA1–BARD1, not shown. **d**, Quantitation of DNA protection assays such as shown in Extended Data Fig. 9h. Averages shown; error bars, s.e.m.; $n = 3$. The data were normalized to the corresponding reaction without RAD51 (lane 2). Values without normalization are plotted in Extended Data Fig. 9i. **e**, Representative protection assays with WRN (25 nM), DNA2 (25 nM), pCtIP (20 nM) and RPA (215 nM), in the absence or presence of BRCA1–BARD1 and either human RAD51 (*Hs*RAD51) or yeast Rad51 (*Sc*Rad51). Top, quantitation of DNA degradation. Averages shown; error bars, s.e.m.; $n = 5$ for reactions containing *Hs*RAD51, in the presence or absence of BRCA1–BARD1 and $n = 3$ for reactions containing *Sc*RAD51, in the presence or absence of BRCA1–BARD1. ****$P \leq 0.0001$, two-tailed t-test. Source data are provided in Supplementary Fig. 3.

Data Fig. 8j). To overcome the lethality caused by CtIP loss, RPE1 *EXO1*$^{+/+}$ or *EXO1*$^{-/-}$ cells were also depleted for TP53. We then monitored cellular survival and observed that the CtIP-S327A mutant reduced the viability of EXO1-deficient but not EXO1-proficient cells (Fig. 5f). Furthermore, using U2OS-derived cells, we observed that C5-dependent inhibition of DNA2 reduced DNA end resection in CtIP wild-type cells but not in CtIP-S327A cells, as monitored by RPA-positive cells upon ionizing radiation (Fig. 5g and Extended Data Fig. 8k,l). We propose that wild-type CtIP channels the resection to the DNA2 pathway through the interactions with DNA2 and BRCA1, and DNA2 inhibition consequently impairs resection. By contrast, in CtIP-S327A cells, the resection primarily proceeds by means of the EXO1 pathway, and DNA2 inhibition is less consequential. These experiments support our conclusions that the CtIP–BRCA1 complex promotes resection primarily by the DNA2 pathway, in agreement with previous observations that CtIP and BRCA1 promote resection speed[16].

RAD51 and BRCA1–BARD1 protect DNA

Independently of their roles in recombination, BRCA1, BRCA2 and RAD51, the main eukaryotic recombinase, as well as many extra cofactors, were shown to prevent unscheduled nascent DNA degradation at challenged DNA replication forks, which may regulate the response of BRCA-deficient tumours to chemotherapy and poly(ADP-ribose) polymerase inhibitors[1,4–7]. Mechanistically, upon replication stress, RAD51 first facilitates replication fork reversal, which may involve its recombinase activity[47]. Subsequently, RAD51 protects nascent DNA[7], which is probably a structural, recombinase-independent function that depends on its ability to bind dsDNA to prevent nuclease access[48]. The involvement of BRCA1 in DNA protection has been puzzling due to its pro-resection function at DSBs, in particular because both processes involve the same nucleases[1]. We set out to test for the effect of RAD51 in the reconstituted DNA resection assays with BRCA1–BARD1 (Extended Data Fig. 9a). In the absence of RAD51, BRCA1–BARD1 promoted DNA end resection by WRN-DNA2-RPA (Fig. 6a). In the presence of RAD51, which partially inhibited resection per se[48], BRCA1–BARD1 enhanced this inhibitory effect (Fig. 6a). DNA protection by BRCA1–BARD1 and RAD51 was observed also with pCtIP (Fig. 6a and Extended Data Fig. 9b), and in kinetic experiments (Extended Data Fig. 9c). Inhibition of resection by RAD51 and BRCA1 was also found in the absence of BARD1 (Extended Data Fig. 9d,e). The inhibitory effect of RAD51 on DNA end resection was dependent on RAD51 capacity to bind DNA (Extended Data Fig. 9a,f). The RAD51 variant K133R, which forms more stable nucleoprotein filaments than wild-type RAD51, was more protective, whereas RAD51 variants K133A and T131P that are less efficient in DNA binding were correspondingly less protective (Extended Data Fig. 9a,f), in agreement with previous data[48].

Compared to the reactions in previous figures, the assays in Fig. 6a and related Extended Data figures were carried out with higher BRCA1–BARD1 concentrations and at higher ionic strength. Using conditions

resembling those used in Figs. 1–4, the stimulatory effect of BRCA1–BARD1 on DNA end resection, in reactions without RAD51, was more apparent (Fig. 6b,c and Extended Data Fig. 9g). RAD51 was inhibitory, and notably more so in the presence of BRCA1–BARD1, again arguing that BRCA1–BARD1 enhances the DNA protection effect of RAD51 (Fig. 6b,c and Extended Data Fig. 9g). By contrast, BRCA1–BARD1 did not affect the inhibitory effect of RAD51 on EXO1 (Fig. 6d and Extended Data Fig. 9h,i). BRCA1–BARD1 also did not affect the RAD51 capacity to protect ssDNA degradation by DNA2 (Extended Data Fig. 10a). Furthermore, whereas human RAD51 (*Hs*RAD51, at 500 nM) was inhibitory when used on top of BRCA1–BARD1-WRN-DNA2-pCtIP-RPA, yeast Rad51 (*Sc*Rad51, at 700 nM) did not inhibit resection (Fig. 6e). The reactions in Fig. 6e used equivalent specific activities of human RAD51 versus yeast Rad51, as determined by their ability to protect DNA against non-cognate endonucleases ScaI and SspI (Extended Data Fig. 10b–d). BRCA1–BARD1 also did not affect the capacity of yeast or human RAD51 to protect DNA from a non-cognate exonuclease ExoIII (Extended Data Fig. 10e). We thus conclude that RAD51 counteracts the nuclease-stimulatory effect of BRCA1–BARD1 and protects DNA in a partially species-specific manner (Extended Data Fig. 10f). It was reported that higher RAD51 concentrations are necessary for fork protection compared to fork reversal[49], highlighting the need for RAD51 cofactors, such as BRCA2, RADX and the RAD51 paralogues to control its levels on DNA to regulate DNA metabolism in various physiological contexts[2,3,6–8,49].

Discussion

We demonstrate that BRCA1–BARD1 directly promotes both DNA2 and EXO1-dependent long-range DNA end resection pathways (Extended Data Figs. 7g and 8i). In the DNA2 branch, BRCA1–BARD1 primarily activates the WRN or BLM helicase component. We found that the stimulatory effect of BRCA1–BARD1 on the DNA2 branch is most apparent when BRCA1–BARD1 is together with pCtIP and MRN, forming the BRCA1–C complex[17,20] (Extended Data Fig. 7g). Consequently, a mutation in pCtIP (S327A), which selectively disrupts the integrity of the BRCA1–C complex[19–21], strongly impairs the stimulation of WRN-DNA2-RPA. BRCA1–C is thus a functionally integrated multi-protein ensemble that directly stimulates resection by WRN/BLM-DNA2-RPA. We instead failed to find a role for the BRCA1 and CtIP interaction in the stimulation of EXO1- or MRN-dependent resection branches. We propose that the more efficient and faster DNA end resection in the presence of BRCA1–BARD1 is better capable to counteract the effectors of 53BP1, such as the Shieldin complex that may obstruct resection[13,15], or the CST complex/Polα-mediated fill-in synthesis at DNA ends[14,50]. BRCA1–BARD1 forms a super-complex together with BRCA2-DSS1, mediated by PALB2 (refs. 2,3,8). Having established that BRCA1 directly promotes DNA end resection, together with previous data demonstrating a role of BRCA1 and/or BRCA2 and cofactors in the activation of RAD51 loading and DNA strand exchange[3,8], it is tempting to speculate that the BRCA1–BRCA2 super-complex may comprehensively regulate and couple the individual initial steps of the homologous recombination pathway.

Online content

Any methods, additional references, Nature Portfolio reporting summaries, source data, extended data, supplementary information, acknowledgements, peer review information; details of author contributions and competing interests; and statements of data and code availability are available at https://doi.org/10.1038/s41586-024-07909-9.

1. Cejka, P. & Symington, L. S. DNA end resection: mechanism and control. *Annu. Rev. Genet.* **55**, 285–307 (2021).
2. Kawale, A. S. & Sung, P. Mechanism and significance of chromosome damage repair by homologous recombination. *Essays Biochem*. https://doi.org/10.1042/EBC20190093 (2020).
3. Prakash, R., Zhang, Y., Feng, W. & Jasin, M. Homologous recombination and human health: the roles of BRCA1, BRCA2, and associated proteins. *Cold Spring Harb. Perspect. Biol.* **7**, a016600 (2015).
4. Schlacher, K., Wu, H. & Jasin, M. A distinct replication fork protection pathway connects Fanconi anemia tumor suppressors to RAD51-BRCA1/2. *Cancer Cell* **22**, 106–116 (2012).
5. Schlacher, K. et al. Double-strand break repair-independent role for BRCA2 in blocking stalled replication fork degradation by MRE11. *Cell* **145**, 529–542 (2011).
6. Ray Chaudhuri, A. et al. Replication fork stability confers chemoresistance in BRCA-deficient cells. *Nature* **535**, 382–387 (2016).
7. Berti, M., Cortez, D. & Lopes, M. The plasticity of DNA replication forks in response to clinically relevant genotoxic stress. *Nat. Rev. Mol. Cell Biol.* **21**, 633–651 (2020).
8. Tarsounas, M. & Sung, P. The antitumorigenic roles of BRCA1-BARD1 in DNA repair and replication. *Nat. Rev. Mol. Cell Biol.* **21**, 284–299 (2020).
9. Stark, J. M., Pierce, A. J., Oh, J., Pastink, A. & Jasin, M. Genetic steps of mammalian homologous repair with distinct mutagenic consequences. *Mol. Cell. Biol.* **24**, 9305–9316 (2004).
10. Polato, F. et al. CtIP-mediated resection is essential for viability and can operate independently of BRCA1. *J. Exp. Med.* **211**, 1027–1036 (2014).
11. Bunting, S. F. et al. 53BP1 inhibits homologous recombination in Brca1-deficient cells by blocking resection of DNA breaks. *Cell* **141**, 243–254 (2010).
12. Bouwman, P. et al. 53BP1 loss rescues BRCA1 deficiency and is associated with triple-negative and BRCA-mutated breast cancers. *Nat. Struct. Mol. Biol.* **17**, 688–695 (2010).
13. Noordermeer, S. M. et al. The shieldin complex mediates 53BP1-dependent DNA repair. *Nature* **560**, 117–121 (2018).
14. Mirman, Z. et al. 53BP1-RIF1-shieldin counteracts DSB resection through CST- and Polalpha-dependent fill-in. *Nature* **560**, 112–116 (2018).
15. Dev, H. et al. Shieldin complex promotes DNA end-joining and counters homologous recombination in BRCA1-null cells. *Nat. Cell Biol.* **20**, 954–965 (2018).
16. Cruz-Garcia, A., Lopez-Saavedra, A. & Huertas, P. BRCA1 accelerates CtIP-mediated DNA-end resection. *Cell Rep.* **9**, 451–459 (2014).
17. Chen, L., Nievera, C. J., Lee, A. Y. & Wu, X. Cell cycle-dependent complex formation of BRCA1.CtIP.MRN is important for DNA double-strand break repair. *J. Biol. Chem.* **283**, 7713–7720 (2008).
18. Wang, B. BRCA1 tumor suppressor network: focusing on its tail. *Cell Biosci.* **2**, 6 (2012).
19. Wong, A. K. et al. Characterization of a carboxy-terminal BRCA1 interacting protein. *Oncogene* **17**, 2279–2285 (1998).
20. Yu, X., Wu, L. C., Bowcock, A. M., Aronheim, A. & Baer, R. The C-terminal (BRCT) domains of BRCA1 interact in vivo with CtIP, a protein implicated in the CtBP pathway of transcriptional repression. *J. Biol. Chem.* **273**, 25388–25392 (1998).
21. Yu, X. & Chen, J. DNA damage-induced cell cycle checkpoint control requires CtIP, a phosphorylation-dependent binding partner of BRCA1 C-terminal domains. *Mol. Cell. Biol.* **24**, 9478–9486 (2004).
22. Gravel, S., Chapman, J. R., Magill, C. & Jackson, S. P. DNA helicases Sgs1 and BLM promote DNA double-strand break resection. *Genes Dev.* **22**, 2767–2772 (2008).
23. Anand, R., Ranjha, L., Cannavo, E. & Cejka, P. Phosphorylated CtIP functions as a co-factor of the MRE11-RAD50-NBS1 endonuclease in DNA end resection. *Mol. Cell* **64**, 940–950 (2016).
24. Nimonkar, A. V. et al. BLM-DNA2-RPA-MRN and EXO1-BLM-RPA-MRN constitute two DNA end resection machineries for human DNA break repair. *Genes Dev.* **25**, 350–362 (2011).
25. Sturzenegger, A. et al. DNA2 cooperates with the WRN and BLM RecQ helicases to mediate long-range DNA end resection in human cells. *J. Biol. Chem.* **289**, 27314–27326 (2014).
26. Cannavo, E., Cejka, P. & Kowalczykowski, S. C. Relationship of DNA degradation by *Saccharomyces cerevisiae* exonuclease 1 and its stimulation by RPA and Mre11-Rad50-Xrs2 to DNA end resection. *Proc. Natl Acad. Sci. USA* **110**, E1661–E1668 (2013).
27. Ceppi, I. et al. CtIP promotes the motor activity of DNA2 to accelerate long-range DNA end resection. *Proc. Natl Acad. Sci. USA* **117**, 8859–8869 (2020).
28. Ceppi, I. et al. PLK1 regulates CtIP and DNA2 interplay in long-range DNA end resection. *Genes Dev.* **37**, 119–135 (2023).
29. Daley, J. M. et al. Enhancement of BLM-DNA2-mediated long-range DNA end resection by CtIP. *Cell Rep.* **21**, 324–332 (2017).
30. Whelan, D. R. & Rothenberg, E. Super-resolution mapping of cellular double-strand break resection complexes during homologous recombination. *Proc. Natl Acad. Sci. USA* https://doi.org/10.1073/pnas.2021963118 (2021).
31. Wang, H. et al. The interaction of CtIP and Nbs1 connects CDK and ATM to regulate HR-mediated double-strand break repair. *PLoS Genet.* **9**, e1003277 (2013).
32. Yun, M. H. & Hiom, K. CtIP-BRCA1 modulates the choice of DNA double-strand-break repair pathway throughout the cell cycle. *Nature* **459**, 460–463 (2009).
33. Nakamura, K. et al. Collaborative action of Brca1 and CtIP in elimination of covalent modifications from double-strand breaks to facilitate subsequent break repair. *PLoS Genet.* **6**, e1000828 (2010).
34. Reczek, C. R., Szabolcs, M., Stark, J. M., Ludwig, T. & Baer, R. The interaction between CtIP and BRCA1 is not essential for resection-mediated DNA repair or tumor suppression. *J. Cell Biol.* **201**, 693–707 (2013).
35. Pinto, C., Kasaciunaite, K., Seidel, R. & Cejka, P. Human DNA2 possesses a cryptic DNA unwinding activity that functionally integrates with BLM or WRN helicases. *eLife* https://doi.org/10.7554/eLife.18574 (2016).
36. Cheng, W. H. et al. Collaboration of Werner syndrome protein and BRCA1 in cellular responses to DNA interstrand cross-links. *Nucleic Acids Res.* **34**, 2751–2760 (2006).
37. Kasaciunaite, K. et al. Competing interaction partners modulate the activity of Sgs1 helicase during DNA end resection. *EMBO J.* **38**, e101516 (2019).
38. Levikova, M., Pinto, C. & Cejka, P. The motor activity of DNA2 functions as an ssDNA translocase to promote DNA end resection. *Genes Dev.* **31**, 493–502 (2017).
39. Miller, A. S. et al. A novel role of the Dna2 translocase function in DNA break resection. *Genes Dev.* **31**, 503–510 (2017).

40. Hoa, N. N. et al. BRCA1 and CtIP are both required to recruit Dna2 at double-strand breaks in homologous recombination. *PLoS ONE* **10**, e0124495 (2015).
41. Oz, R. et al. Phosphorylated CtIP bridges DNA to promote annealing of broken ends. *Proc. Natl Acad. Sci. USA* **117**, 21403–21412 (2020).
42. Zhao, W. et al. BRCA1-BARD1 promotes RAD51-mediated homologous DNA pairing. *Nature* **550**, 360–365 (2017).
43. Parameswaran, B. et al. Damage-induced BRCA1 phosphorylation by Chk2 contributes to the timing of end resection. *Cell Cycle* **14**, 437–448 (2015).
44. Tsukada, K. et al. BLM and BRCA1-BARD1 coordinate complementary mechanisms of joint DNA molecule resolution. *Mol. Cell* **84**, 640–658 e610 (2024).
45. van de Kooij, B. et al. EXO1 protects BRCA1-deficient cells against toxic DNA lesions. *Mol. Cell* **84**, 659–674 e657 (2024).
46. Garcia-Rodriguez, N., Dominguez-Garcia, I., Dominguez-Perez, M. D. C. & Huertas, P. EXO1 and DNA2-mediated ssDNA gap expansion is essential for ATR activation and to maintain viability in BRCA1-deficient cells. *Nucleic Acids Res*. https://doi.org/10.1093/nar/gkae317 (2024).
47. Liu, W. et al. RAD51 bypasses the CMG helicase to promote replication fork reversal. *Science* **380**, 382–387 (2023).
48. Halder, S. et al. Double-stranded DNA binding function of RAD51 in DNA protection and its regulation by BRCA2. *Mol. Cell* **82**, 3553–3565 e3555 (2022).
49. Bhat, K. P. et al. RADX modulates RAD51 activity to control replication fork protection. *Cell Rep.* **24**, 538–545 (2018).
50. Mirman, Z., Sasi, N. K., King, A., Chapman, J. R. & de Lange, T. 53BP1-shieldin-dependent DSB processing in BRCA1-deficient cells requires CST-Polalpha-primase fill-in synthesis. *Nat. Cell Biol.* **24**, 51–61 (2022).

Methods

Cloning, expression and purification of recombinant proteins

Human wild-type DNA2, helicase-dead DNA2 K654R and nuclease-dead DNA2 D277A were expressed in *Sf*9 insect cells and purified by affinity chromatography taking advantage of the N-terminal 6×His tag and the C-terminal FLAG tag[35]. Yeast nuclease-dead Dna2 E675A was expressed in *S. cerevisiae* and purified using the N-terminal FLAG tag and the C-terminal 6×His tag[51]. Full-length wild-type WRN, helicase-dead WRN K577M, exonuclease-dead WRN E84A, WRN fragments, BLM, as well as wild-type CtIP and its variants were purified exploiting the MBP tag at the N terminus and 10×His tag at the C terminus[23,28,35,38,52,53]. The MBP tag was removed during purification by cleavage with PreScission protease. For the expression of phosphorylated wild-type CtIP (pCtIP) and its variants, *Sf*9 cells were treated with 50 nM Okadaic acid (APExBIO) 3 h before collection to preserve the phosphorylated state of the proteins, and 1 μM camptothecin (Sigma) 1 h before collection to increase the activation of the protein phosphorylation cascade. For the expression of dephosphorylated WRN (λWRN) and CtIP (λCtIP), proteins were incubated with λ phosphatase at room temperature for 30 min during purification. The MRN and MRE11–RAD50 complexes were obtained using the 6×His tag and 3×FLAG tag at the C termini of MRE11 and RAD50, respectively[23]. Human wild-type EXO1, as well as nuclease-dead EXO1 D173A, were purified using M2 anti-FLAG affinity resin (Sigma) and HiTrap SP HP cation exchange chromatography column (Cytiva)[26,54]. EXO1Δ1 (Δ353–846) fragment, along with a matched wild-type control, were purified omitting the HiTrap SP HP cation exchange chromatography step. *E. coli* ExoIII, ScaI and SspI were purchased from New England Biolabs. Wild-type human RAD51, as well as the indicated human RAD51 variants and yeast Rad51, were expressed in BL21 (DE3)pLysS *E. coli* cells and purified using amylose affinity chromatography followed by HiTrap Q chromatography (Cytiva)[48].

The *BRCA1* sequence was codon optimized for the expression in *Sf*9 cells (Biomatik) with flanked NheI and XmaI restriction sites. The full-length sequence is listed in Supplementary Table 1 provided in the Supplementary Information. The *BRCA1* gene was then cloned into pFB-2×MBP-CtIP-10×His[55] to generate pFB-2×MBP-BRCA1co-10×His. The cloning created a fusion construct with the 2×MBP tag at the N terminus and the 10×His tag at the C terminus. All BRCA1 variants were cloned from pFB-2×MBP-BRCA1co-10×His using the primers listed in Supplementary Table 3 provided in the Supplementary Information. Similarly, the *BARD1* sequence was codon optimized for the expression in *Sf*9 cells (Supplementary Table 2 provided in the Supplementary Information, Biomatik) with BamHI and XmaI restriction sites. The *BARD1* gene was then cloned into pFB-RAD50co-FLAG[23] to generate pFB-BARD1co-FLAG (BARD1 with C-terminal FLAG tag). All BARD1 variants were cloned from pFB-BARD1co-FLAG using the primers listed in Supplementary Table 3 provided in the Supplementary Information. The BRCA1–BARD1 complex, BRCA1 on its own and all variants were expressed in *Sf*9 cells using the SFX Insect serum-free medium (Hyclone) and the Bac-to-Bac expression system (Invitrogen), according to the manufacturer's recommendations. Frozen *Sf*9 pellets from 1 l of culture were resuspended in lysis buffer (50 mM Tris-HCl pH 7.5, 1 mM ethylenediaminetetraacetic (EDTA), 1:400 protease inhibitor cocktail (Sigma, P8340), 30 μg ml^{-1} leupeptin (Merck Millipore), 1 mM phenylmethylsulfonyl fluoride (PMSF), 1 mM dithiothreitol (DTT), 0.5% NP40) and incubated at 4 °C for 20 min. Glycerol was added to a final concentration of 25%, NaCl was added to a final concentration of 325 mM and the cell suspension was incubated at 4 °C for 20 min. The cell suspension was centrifuged at 55,000*g* at 4 °C for 30 min. The soluble extract was incubated with amylose resin (New England Biolabs) at 4 °C for 1 h. The resin was washed with amylose wash buffer (50 mM Tris-HCl pH 7.5, 2 mM β-mercaptoethanol, 300 mM NaCl, 10% glycerol, 1 mM PMSF). Proteins were eluted using amylose elution buffer (50 mM Tris-HCl pH 7.5, 2 mM β-mercaptoethanol, 300 mM NaCl, 10% glycerol, 1 mM PMSF, 10 mM maltose (Sigma), 20 mM imidazole (Sigma)). The solution was immediately loaded onto pre-equilibrated Ni-NTA agarose resin (Qiagen) at 4 °C, in flow. The resin was washed with Ni-NTA buffer 1 (50 mM Tris-HCl pH 7.5, 2 mM β-mercaptoethanol, 10% glycerol, 1 mM PMSF, 20 mM imidazole and 1 M NaCl for BRCA1 or 0.3 M NaCl for BRCA1–BARD1), and subsequently with Ni-NTA buffer 2 (50 mM Tris-HCl pH 7.5, 2 mM β-mercaptoethanol, 150 mM NaCl, 10% glycerol, 1 mM PMSF, 20 mM imidazole). Proteins were eluted with Ni-NTA elution buffer (50 mM Tris-HCl pH 7.5, 2 mM β-mercaptoethanol, 150 mM NaCl, 10% glycerol, 1 mM PMSF, 200 mM imidazole). Fractions containing high protein concentration as estimated by the Bradford assay were pooled, aliquoted, snap-frozen in liquid nitrogen and stored at −80 °C. The BRCA1–BARD1 mutants were purified in the same way. We note that attempts to cleave the MBP tag before Ni-NTA purification resulted in protein precipitation. We could obtain up to roughly 0.6 mg of BRCA1–BARD1 from 1 l of media (approximate stock concentration, 800 nM). For the expression of dephosphorylated BRCA1–BARD1 (λBRCA1–BARD1), the complex was incubated with λ phosphatase at room temperature for 30 min during purification, along with a matched control that was similarly incubated but without λ phosphatase.

Human *RPA* sequence was cloned from p11d–tRPA construct[56] using the primers listed in Supplementary Table 3 provided in the Supplementary Information. Whereas both RPA1 and RPA2 were flanked by the BamHI and NheI restriction sites, RPA3 was flanked by SalI and XbaI. These restriction enzymes were used to generate pFB-RPA1, pFB-RPA2 and pFB-6×His-RPA3 insect expression vectors used for the protein purification. RPA was expressed in *Sf*9 cells in SFX Insect serum-free medium (Hyclone) using the Bac-to-Bac expression system (Invitrogen), according to the manufacturer's recommendations. A frozen *Sf*9 pellet from 2 l of culture was resuspended in lysis buffer (50 mM Tris-HCl pH 7.5, 2 mM β-mercaptoethanol, 1:200 protease inhibitor cocktail, 60 μg ml^{-1} leupeptin, 1 mM PMSF, 20 mM imidazole, 0.1% NP40) and incubated at 4 °C for 20 min. Glycerol was added to a final concentration of 25%, KCl was added to a final concentration of 325 mM and the cell suspension was incubated at 4 °C for 30 min. The cell suspension was centrifuged at 55,000*g* at 4 °C for 30 min. The soluble extract was incubated with Ni-NTA affinity resin at 4 °C for 1 h. Ni-NTA resin was washed with wash buffer (50 mM Tris-HCl pH 7.5, 2 mM β-mercaptoethanol, 1 mM PMSF, 10% glycerol, 500 mM KCl, 20 mM imidazole, 0.1% NP40). Protein was eluted using wash buffer containing 300 mM imidazole. The eluate was diluted by adding 2 volumes of buffer A (30 mM HEPES pH 7.5, 1 mM DTT, 1 mM PMSF, 10% glycerol, 500 mM KCl, 0.25 mM EDTA, 0.01% NP40). The diluted fractions were purified on a HiTrap Blue HP column (Cytiva) followed by HiTrap desalting column (Cytiva) as described[57]. Peak desalted fractions were pooled, diluted with 1 volume of buffer B (30 mM HEPES pH 7.5, 1 mM DTT, 1 mM PMSF, 10% glycerol, 0.25 mM EDTA) and loaded onto two 5 ml HiTrap Heparin columns (Cytiva) connected in tandem. Proteins were eluted using a 30 ml gradient of 50 mM to 1 M KCl in 1 ml fractions. Peak fractions were pooled and diluted to a final concentration of roughly 100 mM KCl with buffer B. The diluted eluate was loaded and further purified on a HiTrap Q column (Cytiva) as previously described[57]. We could obtain roughly 45 mg of human RPA from 2 l insect cells. The sequences of all primers used for cloning in this study are listed in Supplementary Table 3 provided in the Supplementary Information. Purified recombinant proteins were analysed by using SDS–PAGE denaturing electrophoresis and stained with Coomassie Brilliant Blue (VWR). The final images were acquired with a photo scanner operated with Epson Scan v.3.9.4.0 US software and CanoScan 9000F Mark II scanner operated with ImageCapture v.6.6(525) software.

The sg*CtIP* (CTCCCGGATCTATACTCCAC) used for depletion of endogenous CtIP in RPE1 *EXO1*$^{+/+}$ and RPE1 *EXO1*$^{-/-}$ cells was cloned into pLentiCRISPR-v2 using BsmBI. The PAM-sequence of this guide RNA (gRNA) was mutated in the full-length pcDNA3.1 CtIP overexpressing constructs (pcDNA3.1_CtIP-WT-2×FLAG and

pcDNA3.1_CtIP-S327A-2×FLAG) using site-directed mutagenesis to render the exogenous CtIP expression insensitive to CRISPR-mediated depletion. Subsequently, the coding sequence was cloned into the Gateway entry vector pENTR_1A using KpnI and NotI before transferring it to the destination vector pCW57.1-Zeo using a Gateway LR reaction.

Sequence analysis of BRCA1 and BARD1 proteins

Alignment of the BRCA1 region 931–1171 and of the BARD1 region 123–261 were generated using the MAFFT method[58] and represented using Jalview[59].

Preparation of DNA substrates

The sequences of all oligonucleotides used for DNA substrate preparation are listed in Supplementary Table 4 provided in the Supplementary Information. The oligonucleotide-based Y-structured DNA substrate was prepared with the oligonucleotides X12-3HJ3 and X12-3TOPLbis[35]. The oligonucleotide-based 70 bp-long dsDNA substrate was prepared with the oligonucleotides PC210 and PC211. X12-3HJ3 and PC210 oligonucleotides were ^{32}P-labelled at the 3′ terminus with (α-^{32}P)dCTP (Hartmann Analytic) and terminal transferase (New England Biolabs) according to the manufacturer's instructions. The oligonucleotide-based 70 bp-long dsDNA biotinylated at the 5′ terminus was prepared using the oligonucleotides PC206 and PC217. PC206 oligonucleotide was ^{32}P-labelled at the 5′ terminus with (γ-^{32}P) ATP (Hartmann Analytic) and T4 PNK (New England Biolabs) according to the manufacturer's instructions. The randomly labelled 2.2 kbp-long substrate was prepared by amplifying the human *NBS1* gene by PCR reaction containing 66 nM (α-^{32}P)dCTP (Hartmann Analytic) with the standard dNTPs concentration (200 μM each)[27]. When randomly labelled ssDNA was required, the 2.2 kbp-long substrate was heated at 95 °C for 5 min before the experiments. The HindIII digest of λ DNA (New England Biolabs) was labelled by fill-in at the 3′ end with (α-^{32}P) dCTP (Hartmann Analytic), dGTP, dATP (0.25 mM each) and 5 U of the Klenow fragment of DNA polymerase I exo- (lacking the 3′–5′ and 5′–3′ exonuclease activities of DNA polymerase I) (New England Biolabs). Unincorporated nucleotides were removed with Micro Bio-Spin P-30 Tris chromatography columns (BioRad). When the heat-denatured substrate was needed, the substrate was incubated at 95 °C for 5 min to obtain ssDNA[27]. pUC19-based dsDNA substrate was prepared by digesting the pUC19 plasmid with HindIII-HF restriction enzyme (New England Biolabs) according to the manufacturer's instructions, and purified by phenol-chloroform extraction and ethanol precipitation. The resulting linear dsDNA was labelled by fill-in at the 3′ end with 0.25 mM of (α-^{32}P)dCTP (Hartmann Analytic), dGTP, dATP and 5 U of the Klenow fragment of DNA polymerase I exo- (New England Biolabs). Unincorporated nucleotides were removed using Micro Bio-Spin P-30 Tris chromatography columns (BioRad). For the ATPase assay with wild-type DNA2 and helicase-dead DNA2 D277A, the 10.3 kbp-long pFB-MBP-hMLH3 plasmid[60] was linearized with NheI (New England Biolabs) and purified with QIAquick PCR purification kit (Qiagen). The substrate was denatured at 95 °C for 5 min to obtain ssDNA. The overhanging substrate used for single-molecule magnetic tweezer experiments was prepared as previously described[61,62]. Briefly, the main 6.6 kbp-long fragment was prepared from pNLRep plasmid[63] using the restriction enzymes BamHI and BsrGI (New England Biolabs). Furthermore, a 63 nt-long ssDNA gap was introduced using the nicking enzyme Nt.BbvCI (New England Biolabs). The gap was then filled by hybridizing a 25 nt-long DNA oligomer carrying an extra 40 nt-long polythimidine tail at the 5′ end (overhang), followed by 3′ end ligation inside the gap. Subsequently, 600 bp-long DNA handles carrying either several digoxigenin or biotin modifications were attached at either end. The handles were produced by PCR using as a template the plasmids pBlueScript II SK+ (digoxigenin, Dig handle Forward and Dig handle Reverse primers) or pNLRep (biotin, Bio handle Forward and Bio handle Reverse primers), respectively, in the presence of digoxigenin and biotin-modified nucleotides and digested with BamHI or BsrGI (New England Biolabs), respectively. The final construct shows the 5′ overhang at roughly 0.5 kbp distance from the surface attachment handle.

DNA end resection and protection assays

DNA endonuclease assays with the MRN complex and pCtIP were performed in 15 μl volume in nuclease buffer containing 25 mM Tris-acetate pH 7.5, 5 mM magnesium acetate, 1 mM manganese acetate, 1 mM ATP, 1 mM DTT, 0.25 mg ml^{-1} bovine serum albumin (BSA) (New England Biolabs), 1 mM phosphoenolpyruvate (PEP), 80 U ml^{-1} pyruvate kinase (Sigma) and 1 nM substrate (in molecules). Biotinylated DNA ends were blocked by adding 15 nM monovalent streptavidin (a kind gift from M. Howarth, University of Oxford)[64] and by incubating the samples at room temperature for 5 min. Different from above, DNA exonuclease assays with recombinant MRE11–RAD50 were carried out in nuclease buffer containing 3 mM manganese acetate. Recombinant proteins were added on ice and the reactions were incubated at 37 °C for 2 h. Reactions were stopped by adding 0.5 μl of 0.5 M EDTA and 1 μl Proteinase K (Roche, 18 mg ml^{-1}), and incubated at 50 °C for 30 min. An equal amount of formamide dye (95% [v/v] formamide, 20 mM EDTA, bromophenol blue) was added, samples were heated at 95 °C for 4 min and separated on 15% denaturing polyacrylamide gels (ratio acrylamide:bisacrylamide 19:1, BioRad). After fixing in a solution containing 40% methanol, 10% acetic acid and 5% glycerol for 30 min, the gels were dried on 3MM paper (Whatman), exposed to storage phosphor screens (GE Healthcare) and scanned with Typhoon FLA 9500 Phosphor Imager (GE Healthcare).

DNA end-resection assays with PCR-based or pUC19-based dsDNA substrate were performed in a 15 μl volume in 25 mM Tris-acetate pH 7.5, 2 mM magnesium acetate, 1 mM ATP, 1 mM DTT, 0.1 mg ml^{-1} BSA, 1 mM PEP, 80 U ml^{-1} pyruvate kinase and 1 nM substrate (in molecules). NaCl was added to the reaction buffer to a final concentration of 50 mM (unless indicated otherwise) taking into account the salt coming from protein storage or dilution buffers. When randomly labelled ssDNA was used, 2 nM substrate (in molecules) was used. Where indicated, AMP-PNP (Toronto Research Chemicals) or ATP-γ-S (Cayman Chemical) were used instead of ATP. Human RPA was included to saturate all ssDNA, as indicated. Further recombinant proteins were then added on ice and the reactions were incubated at 37 °C for 30 min, unless indicated otherwise. Reactions were stopped by adding 5 μl of 2% stop solution (150 mM EDTA, 2% SDS, 30% glycerol, bromophenol blue) and 1 μl of Proteinase K (Roche, 18 mg ml^{-1}) and incubated at 37 °C for 15 min. Samples were analysed by 1% agarose gel electrophoresis. Gels were dried on DE81 chromatography paper (Whatman) and analysed as described above.

The nuclease assays with λ DNA/HindIII-based substrates were carried out similarly as described above with the following differences. DNA was used at 0.15 nM (in molecules), the reaction buffer contained 3 mM magnesium acetate, 30 mM NaCl and, unless indicated otherwise, reactions were incubated at 37 °C for 1 h. DNA protection assays with PCR-based dsDNA substrate were carried out as indicated above for the respective DNA end resection assays, except RAD51, BRCA1–BARD1 or BRCA1 were pre-incubated at 37 °C for 10 min before the addition of the other recombinant proteins. Protection reactions were stopped by adding 0.5 μl of 0.5 M EDTA and 1 μl of Proteinase K (Roche, 18 mg ml^{-1}), and incubated at 50 °C for 30 min. An equal amount of formamide dye (95% [v/v] formamide, 20 mM EDTA, bromophenol blue) was added, and samples were heated at 95 °C for 4 min and separated on 20% denaturing polyacrylamide gels (ratio acrylamide:bisacrylamide 19:1). After fixing in a solution containing 40% methanol, 10% acetic acid and 5% glycerol for 30 min, the gels were dried on 3MM paper (Whatman) and analysed as described above. Protection assays with pUC19-based dsDNA substrate were carried out as indicated above for the respective DNA end resection assays. Signals were quantified using ImageJ2 (National Institutes of Health, NIH) and plotted with Prism 10 (GraphPad).

Helicase assays

Helicase assays with the oligonucleotide-based Y-structured DNA substrate were performed in 15 µl volume in reaction buffer (25 mM Tris-acetate pH 7.5, 5 mM magnesium acetate, 1 mM ATP, 1 mM DTT, 0.1 mg ml^{-1} BSA, 1 mM PEP, 80 U ml^{-1} pyruvate kinase and 50 mM NaCl) with 0.1 nM DNA substrate (in molecules). Recombinant proteins were added as indicated. Reactions were incubated at 37 °C for 30 min and stopped by adding 5 µl of 2% stop solution (150 mM EDTA, 2% SDS, 30% glycerol, bromophenol blue) and 1 µl of Proteinase K (Roche, 18 mg ml^{-1}) and incubated at 37 °C for 10 min. To avoid re-annealing of the substrate, the 2% stop solution was supplemented with a 20-fold excess of the unlabelled oligonucleotide with the same sequence as the ^{32}P-labelled one. The products were separated by 10% polyacrylamide gel electrophoresis, dried on 17 CHR chromatography paper (Whatman) and analysed as described for resection assays. Helicase assays with PCR-based, pUC19-based dsDNA substrate or HindIII digest of λ DNA were performed as described for the respective DNA end resection assays. Signals were quantified using ImageJ2 (NIH) and plotted with Prism 10 (GraphPad).

ATPase assays

ATPase assays with recombinant WRN were performed in 25 mM Tris-acetate pH 7.5, 5 mM magnesium acetate, 1 mM DTT, 0.1 mg ml^{-1} BSA, 1 mM ATP, 100 mM NaCl, 1 nM of (γ-^{32}P)ATP (Hartmann Analytic) and 0.1 nM (in molecules) of the X12-3HJ3 oligonucleotide used to prepare the Y-structured DNA substrate used in the helicase assays. RPA and BRCA1–BARD1 or BRCA1 were added on ice and samples were pre-incubated at 37 °C for 10 min. WRN was then added and reactions were incubated at 37 °C for 30 min. ATPase assays with recombinant wild-type DNA2 and nuclease-dead DNA2 D277A were performed in 25 mM Tris-acetate pH 7.5, 3 mM magnesium acetate, 1 mM DTT, 0.1 mg ml^{-1} BSA, 1 mM ATP, 20 mM NaCl, 1 nM of (γ-^{32}P)ATP (Hartmann Analytic) and 0.32 nM (in molecules) of a heat-denatured 10.3 kbp-long dsDNA as a substrate. RPA and indicated proteins were added on ice and samples were incubated at 37 °C for 15 min. Reactions were stopped with 1.1 µl of 0.5 M EDTA, and separated using thin layer chromatography plates (Merck) with 0.3 M LiCl and 0.3 M formic acid as the mobile phase. Dried plates were exposed to storage phosphor screens (GE Healthcare) and scanned with Typhoon FLA 9500 Phosphor Imager (GE Healthcare). Signals were quantified using ImageJ2 (NIH) and plotted with Prism 10 (GraphPad).

Protein-interaction assays

To test the interaction between BRCA1–BARD1 and WRN or EXO1, 1 µg of anti-BRCA1 antibody (Santa Cruz Biotechnology, sc-6954) or anti-WRN antibody (Cell Signaling, 4666S) were captured on 10 µl Protein G magnetic beads (Dynabeads, Invitrogen) by incubating at 4 °C for 1 h with gentle rotation in 50 µl of PBS-T (PBS with 0.1% Tween-20, Sigma). The beads were washed twice on a magnetic rack with 150 µl of PBS-T. The beads were then mixed with 1 µg of the bait in 60 µl of immunoprecipitation buffer (25 mM Tris-HCl pH 7.5, 1 mM DTT, 3 mM EDTA, 0.20 µg µl^{-1} BSA, 100 mM NaCl) and incubated at 4 °C for 1 h with gentle rotation. Beads were washed three times with 150 µl of wash buffer (25 mM Tris-HCl pH 7.5, 1 mM DTT, 3 mM EDTA, 80 mM NaCl, 0.05% Triton-X, Sigma). Then 1 µg of the prey was added to the beads in 60 µl of immunoprecipitation buffer (25 mM Tris-HCl pH 7.5, 1 mM DTT, 3 mM EDTA, 0.20 µg µl^{-1} BSA, 100 mM NaCl) and incubated at 4 °C for 1 h with gentle rotation. Beads were again washed three times with 150 µl of wash buffer (25 mM Tris-HCl pH 7.5, 1 mM DTT, 3 mM EDTA, 80 mM NaCl, 0.05% Triton-X) and proteins were eluted by boiling the beads in SDS buffer (50 mM Tris-HCl pH 6.8, 1.6% SDS, 100 mM DTT, 10% glycerol, 0.01% bromophenol blue) at 95 °C for 3 min. Avidin (Sigma) was added to the eluate as a stabilizer. The eluate was separated on a 7.5% SDS–PAGE gel and proteins were detected by western blotting using anti-BRCA1 antibody (Santa Cruz Biotechnology, sc-6954, 1:1,000), anti-His antibody (Invitrogen PA1-983B, 1:1,000) or anti-FLAG antibody (Sigma, F3165, 1:1,000). The final images were acquired with Fusion FX7 capture software (Vilber Imaging).

Mass photometry characterization of protein complexes

Mass photometry measurements were performed on a TwoMP mass photometer (Refeyn Ltd). First, borosilicate microscope glass plate (No. 1.5 H thickness, 24 × 50 mm, VWR) were cleaned by sequential soaking in Milli-Q-water, isopropanol and Milli-Q-water followed by drying under a stream of clean nitrogen. Next, silicone gaskets (CultureWell Reusable Gasket, Grace Bio-Labs) were placed on the clean coverslip to create a defined well for sample delivery. To convert optical reflection-interference contrast into a molecular mass, a known protein size marker (NativeMark Unstained Protein Standard, Invitrogen) was measured on the same day. For mass measurements, gaskets were filled with 18 µl of measurement buffer (25 mM Tris-HCl pH 7.5, 1 mM ATP, 3 mM magnesium acetate) to allow focusing the microscope onto the coverslip surface. Subsequently, 40 nM of either BRCA1 or BRCA1–BARD1 were added into the well (final volume, 20 µl) and sample binding to the coverslip surface was monitored for 1 min using the software AcquireMP (Refeyn Ltd). Data analysis was performed using DiscoverMP software (Refeyn Ltd).

Single-molecule magnetic tweezer experiments

Single-molecule magnetic tweezer experiments were carried out in a custom-built magnetic tweezers setup and operated using a self-developed code in Labview (2016, National Instruments)[65]. The DNA constructs were linked at their biotinylated ends with streptavidin-coated magnetic beads (Dynabeads M280, Thermo Fisher Scientific) and flushed into the flow cell, where the bottom slide was coated with antidigoxigenin to ensure surface-specific binding. Moving the magnet closer to the flow cell resulted in the stretching of the DNA molecules that were attached to a magnetic bead. Tracking of the magnetic beads for all measurements was conducted at 300 Hz using video microscopy and real-time GPU-accelerated image analysis[66]. The magnetic forces were calibrated based on fluctuation analysis[67]. The measurements were performed in a reaction buffer (25 mM Tris-acetate pH 7.5, 2 mM magnesium acetate, 1 mM ATP, 1 mM DTT, 0.1 mg ml^{-1} BSA), with the indicated protein concentrations at a temperature of 37 °C and forces between 15 and 25 pN. The analysis of the recorded traces was conducted with a custom written MATLAB program[68]. We considered only traces from measurements in which the magnetic bead position was traceable for at least 300 s. The acquired processivity and velocity for the unwinding events were calculated by fitting linear segments to parts of the recorded traces with roughly constant velocity, which were used to construct the histograms and for statistical analysis. To quantify the ratio of rewinding/unwinding events, the total number of the two events, acquired as described above, was determined for a fixed period of 300 s for each recorded trace. To characterize the different protein combinations (Fig. 3c) and WRN variants (Extended Data Fig. 7e), the difference between the maximum value and the minimum value of DNA extension for a given molecule was calculated during the first 300 s and expressed as ΔDNA-length. Each dot represents one measured molecule.

Cell lines

The RPE1 hTERT were purchased from American Type Culture Collection (ATCC). The RPE1 hTERT *PAC*$^{-/-}$*TP53*$^{-/-}$ cell line (referred to as RPE1 *EXO1*$^{+/+}$ in this paper)[45] was used to generate RPE1 hTERT *PAC*$^{-/-}$*TP53*$^{-/-}$ *EXO1*$^{-/-}$ (referred to as RPE1 *EXO1*$^{-/-}$) cells by nucleofection of pLentiCRISPR_v2 containing the sg*EXO1* (GCGTGGGATTGGATTAGCAA) as described before[45]. After clonal selection, genotyping was performed to confirm indel formation using target locus PCR amplification and Sanger sequencing, followed by TIDE (tracking of indels by decomposition) analysis. RPE1 *EXO1*$^{+/+}$ and *EXO1*$^{-/-}$ cells inducibly expressing

exogenous CtIP-WT or CtIP-S327A were obtained by viral transduction with pCW57.1_Zeo-CtIP-WT-2×FLAG or pCW57.1_Zeo-CtIP-S327A-2×FLAG.

U2OS cells were originally bought from ATCC. U2OS-derived cells, carrying green fluorescent protein (GFP), GFP-CtIP-WT or GFP-CtIP-S327A mutant[16], were grown in DMEM medium (Sigma). Media were supplemented with 10% fetal bovine serum (Sigma), 2 mM L-glutamine (Sigma), 100 U ml^{-1} penicillin and 100 µg ml^{-1} streptomycin (Sigma). U2OS cells were last authenticated in June 2024 by the GenePrint 10 System (Promega) using short tandem repeat profiling, and data were analysed using genemapper id-x v.1.2 software (Applied Biosystems) at the genomic core facility of the Instituto de Investigaciones Biomedicas Sols-Morreale. All cell lines were routinely tested for mycoplasm contamination. All the experiments performed here used mycoplasm-free cell lines.

Viral transductions and transfections

Third-generation packaging vectors pMDLg/pRRE, pRSV-Rev, pMD2.g and a lentiviral expression vector (pLentiCRISPR-v2 or pCW57.1) were transfected to human embryonic kidney (HEK) 293T using jet-PEI (Polyplus Transfection) to produce lentiviral particles. The HEK 293T cell line was originally purchased from ATCC. The medium was refreshed 16 h post-transfection. Viral supernatants were harvested 48 h post-transfection, filtered with a 0.45 mm filter and transduced into cells at a multiplicity of infection of 1 in the presence of 4 µg ml^{-1} polybrene. Puromycin (2 µg ml^{-1}) and zeocin (400 µg ml^{-1}) were used for the selection of pLentiCRISPR- and pCW57.1- transduced RPE1 cells, respectively.

Clonogenic survival assays

RPE1 *EXO1*$^{+/+}$ or *EXO1*$^{-/-}$ cells transduced with CtIP-WT or CtIP-S327A were induced with doxycycline (2 µg ml^{-1}) to express CtIP protein exogenously. Cells were virally transduced with pLentiCRISPR-sg*CtIP* or empty vector to deplete endogenous CtIP 24 h post-doxycycline induction. After 48 h of puromycin selection to select for pLentiCRISPR transduced cells, 500 cells were seeded in 10-cm dishes for clonogenic growth. Medium containing doxycycline (2 µg ml^{-1}) was refreshed after 7 days. After 14 days, colonies were stained with crystal violet solution (0.4% [w/v], 20% methanol) and counted manually. Simultaneously with plating cells for clonogenic survival, cells were collected for immunoblotting analysis and lysed in RIPA lysis buffer (1% NP40, 50 mM Tris-HCl pH 7.5, 150 mM NaCl, 0.1% SDS, 3 mM $MgCl_2$, 0.5% sodium deoxycholate) supplemented with Complete Protease Inhibitor Cocktail (Sigma) and 100 U ml^{-1} Benzonase (Sigma). Western blots were stained with primary antibodies against CtIP (Millipore, MABE1060, 1:2,000), FLAG (Sigma, F1804-200UG, 1:2,000), EXO1 (Abcam, ab95068, 1:1,000) and α-Tubulin (Sigma, T6199, 1:5,000); and with HRP-conjugated secondary antibodies donkey anti-rabbit IgG-HRP (Thermo Scientific, 31458, 1:5,000) or goat anti-mouse IgG-HRP (Thermo Scientific, 31432, 1:5,000).

Immunofluorescence and microscopy

For RPA foci visualization, U2OS-derived cells were seeded on coverslips. For the experiment with DNA2 inhibitor C5 (MedChemExpress, catalogue no. HY128729), 20 µM of the inhibitor or the same amount of vehicle (dimethylsulfoxide, DMSO) were added to the plates 6 h before irradiation. Then 1 h after irradiation (10 Gy), coverslips were washed once with PBS followed by treatment with pre-extraction buffer (25 mM Tris-HCl pH 7.5, 50 mM NaCl, 1 mM EDTA, 3 mM $MgCl_2$, 300 mM sucrose and 0.2% Triton-X-100) for 5 min on ice. Cells were fixed with 4% paraformaldehyde [w/v] in PBS for 20 min. Following two washes with PBS, cells were blocked for 1 h with 5% fetal bovine serum in PBS, costained with the appropriate primary antibodies (RPA2, Abcam, ab2175, 1:500) in blocking solution overnight at 4 °C or for 2 h at room temperature, washed again with PBS and then co-immuno-stained with the appropriate secondary antibodies (Alexa Fluor 594 goat anti-mouse, Invitrogen, A11032, 1:500 and Alexa Fluor 488 goat anti-rabbit, Invitrogen, A11034, 1:500) in blocking buffer. After washing with PBS, coverslips were incubated sequentially in 70% and 100% ethanol to dehydrate them. Finally, they were air dried and mounted into glass slides using Vectashield mounting medium with 4,6-diamidino-2-phenylindole (Vector Laboratories). RPA foci immunofluorescence was analysed using a Leica DM6000B Fluorescence microscope (AF6000).

Cell-cycle analysis

Cells were trypsinized and fixed with cold 70% ethanol overnight, incubated with 250 µg ml^{-1} RNase A (Sigma) and 10 µg ml^{-1} propidium iodide (Fluka) at 37 °C for 30 min and analysed with a LSRFortessaTM Cell Analyzer (BD) Flow Cytometer. Cell-cycle distribution data were further analysed using ModFit LT v.5.0 software (Verity Software House Inc.).

Statistics and reproducibility

Sample size or number of technical (for biochemical assays) and biological (for cellular assays) replicates were chosen on the basis of what is common in the field and what was practical to do. A minimum of three independent replicates were performed for each biochemical experiment to add statistical analysis, when required. Where indicated, a representative experiment from independent repeats with similar results was shown. Coomassie-stained protein gels were repeated twice to confirm the quality and the concentration of the indicated recombinant proteins. Protein-interaction assays were performed twice.

Reporting summary

Further information on research design is available in the Nature Portfolio Reporting Summary linked to this article.

Data availability

All relevant data generated or analysed during this study are included in this published Article and its Supplementary Information. Videos underlying mass photometry analysis and single-molecule source data are uploaded to Dryad (https://doi.org/10.5061/dryad.gf1vhhmxc)[69]. Source data are provided with this paper.

51. Acharya, A. et al. Distinct RPA domains promote recruitment and the helicase-nuclease activities of Dna2. *Nat. Commun.* **12**, 6521 (2021).
52. Mengoli, V. et al. WRN helicase and mismatch repair complexes independently and synergistically disrupt cruciform DNA structures. *EMBO J.* **42**, e111998 (2023).
53. Cejka, P. & Kowalczykowski, S. C. The full-length *Saccharomyces cerevisiae* Sgs1 protein is a vigorous DNA helicase that preferentially unwinds holliday junctions. *J. Biol. Chem.* **285**, 8290–8301 (2010).
54. Cannavo, E. et al. Regulation of the MLH1-MLH3 endonuclease in meiosis. *Nature* **586**, 618–622 (2020).
55. Howard, S. M., Ceppi, I., Anand, R., Geiger, R. & Cejka, P. The internal region of CtIP negatively regulates DNA end resection. *Nucleic Acids Res.* **48**, 5485–5498 (2020).
56. Henricksen, L. A., Umbricht, C. B. & Wold, M. S. Recombinant replication protein A: expression, complex formation, and functional characterization. *J. Biol. Chem.* **269**, 11121–11132 (1994).
57. Anand, R., Pinto, C. & Cejka, P. Methods to study DNA end resection I: recombinant protein purification. *Methods Enzymol.* **600**, 25–66 (2018).
58. Katoh, K. & Standley, D. M. MAFFT multiple sequence alignment software version 7: improvements in performance and usability. *Mol. Biol. Evol.* **30**, 772–780 (2013).
59. Waterhouse, A. M., Procter, J. B., Martin, D. M., Clamp, M. & Barton, G. J. Jalview version 2–a multiple sequence alignment editor and analysis workbench. *Bioinformatics* **25**, 1189–1191 (2009).
60. Ranjha, L., Anand, R. & Cejka, P. The *Saccharomyces cerevisiae* Mlh1-Mlh3 heterodimer is an endonuclease that preferentially binds to Holliday junctions. *J. Biol. Chem.* **289**, 5674–5686 (2014).
61. Levikova, M., Klaue, D., Seidel, R. & Cejka, P. Nuclease activity of *Saccharomyces cerevisiae* Dna2 inhibits its potent DNA helicase activity. *Proc. Natl Acad. Sci. USA* **110**, E1992–E2001 (2013).
62. Grigaitis, R. et al. Phosphorylation of the RecQ helicase Sgs1/BLM controls its DNA unwinding activity during meiosis and mitosis. *Dev. Cell* **53**, 706–723 e705 (2020).
63. Luzzietti, N. et al. Efficient preparation of internally modified single-molecule constructs using nicking enzymes. *Nucleic Acids Res.* **39**, e15 (2011).
64. Howarth, M. et al. A monovalent streptavidin with a single femtomolar biotin binding site. *Nat. Methods* **3**, 267–273 (2006).
65. Klaue, D. & Seidel, R. Torsional stiffness of single superparamagnetic microspheres in an external magnetic field. *Phys. Rev. Lett.* **102**, 028302 (2009).

66. Huhle, A. et al. Camera-based three-dimensional real-time particle tracking at kHz rates and Angstrom accuracy. *Nat. Commun.* **6**, 5885 (2015).
67. Daldrop, P., Brutzer, H., Huhle, A., Kauert, D. J. & Seidel, R. Extending the range for force calibration in magnetic tweezers. *Biophys. J.* **108**, 2550–2561 (2015).
68. Kemmerich, F. E., Kasaciunaite, K. & Seidel, R. Modular magnetic tweezers for single-molecule characterizations of helicases. *Methods* **108**, 4–13 (2016).
69. Ceppi, I. et al. Mechanism of BRCA1-BARD1 function in DNA end resection and DNA protection. *Dryad* https://doi.org/10.5061/dryad.gf1vhhmxc (2024).

Acknowledgements We thank members of the Cejka laboratory for their critical comments on this paper. The Swiss National Science Foundation (grant nos. 310030_207588 and 310030_205199) and the European Research Council (grant no. 101018257) support the research in the Cejka laboratory. M.R.D.S. is a recipient of the EMBO Postdoctoral Fellowship (grant no. ALTF-710-2021). Work in the Huertas laboratory was supported by grant no. PID2022-136791NB-I00 funded by grant no. MICIU/AEI/10.13039/501100011033/FEDER/UE. This work is supported by Agence Nationale de la Recherche (grant no. ANR-21-CE44-0009) and by IDRIS (grant no. AD010314343R1) to R.G. Research in the Noordermeer laboratory is funded by the European Union through the MSCA doctoral network Replifate and by Oncode Institute. We thank the Sung laboratory for communicating data before publication.

Author contributions I.C., M.R.D.S. and P.C. designed the study. I.C. and M.R.D.S. prepared most of the recombinant proteins, carried out and analysed most of the experiments. M.M. carried out single-molecule magnetic tweezer experiments with the supervision of R.S. S.B. prepared human RPA and performed resection experiments with human EXO1 and bacterial ExoIII. M.M. and S.B. contributed equally. V.M. prepared some of the truncated WRN protein variants and carried out preliminary unwinding assays. G.R. carried out assays in Extended Data Figs. 1e and 2k,l. H.M.P.V. performed clonogenic survival experiments with the supervision of S.M.N. S.J. carried out immunofluorescence and microscopy analysis of RPA^+ cells with the supervision of P.H. A.A. cloned and contributed to the preparation of all the BRCA1 and BARD1 variants. M.R. purified EXO1 Δ1. A.S. optimized and carried out the preliminary protection assays with WRN, DNA2 and RAD51. S.H. and S.M.H. performed the first BRCA1 and BRCA1–BARD1 protein preparations. R.G. carried out protein alignments and contributed to the design of the BRCA1 and BARD1 variants. I.C., M.R.D.S. and P.C. wrote the paper with contributions from all authors.

Competing interests The authors declare no competing interests.

Additional information
Supplementary information The online version contains supplementary material available at https://doi.org/10.1038/s41586-024-07909-9.
Correspondence and requests for materials should be addressed to Petr Cejka.
Peer review information *Nature* thanks Maria Spies and the other, anonymous, reviewer(s) for their contribution to the peer review of this work. Peer reviewer reports are available.
Reprints and permissions information is available at http://www.nature.com/reprints.

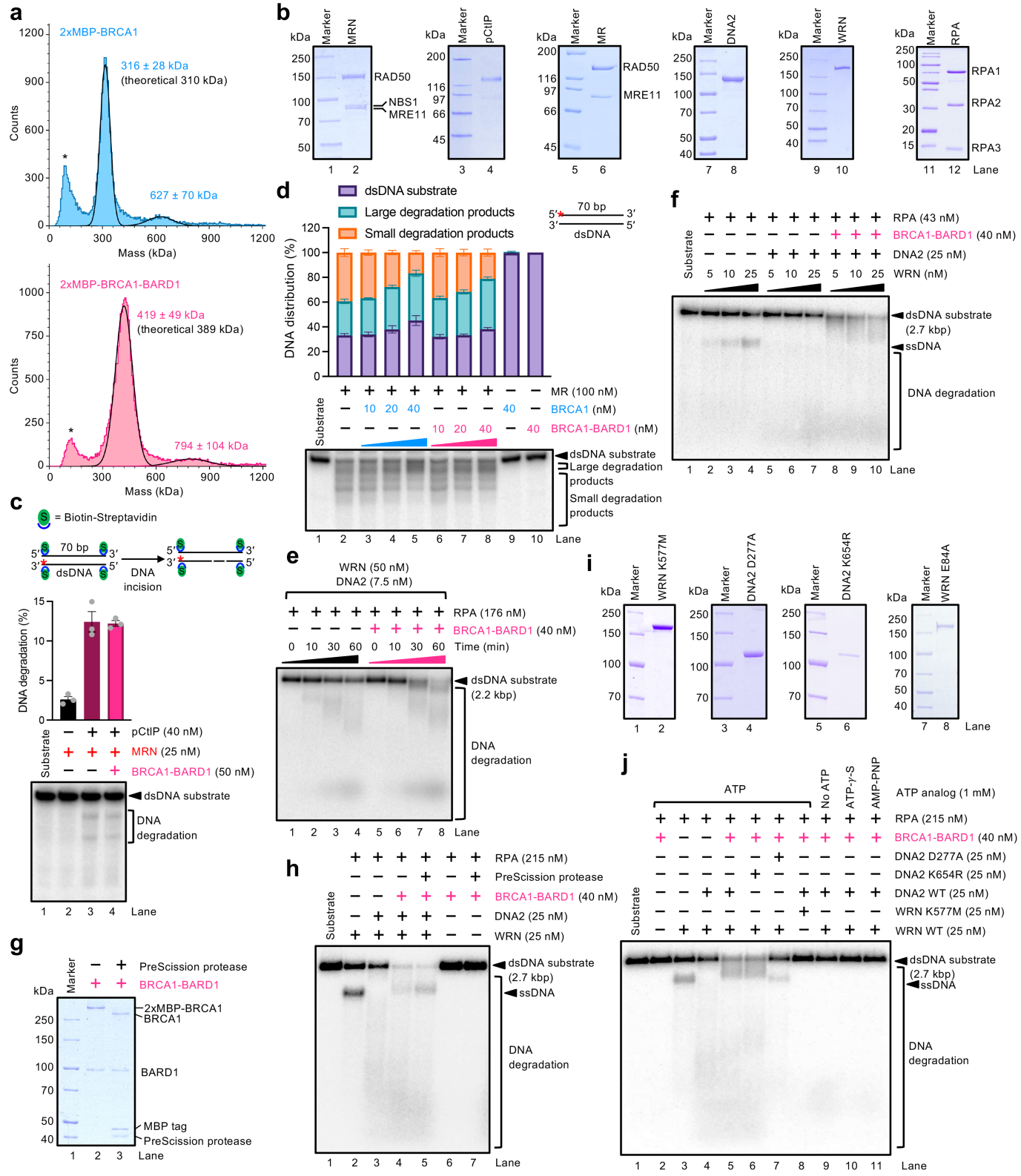

Extended Data Fig. 1 | See next page for caption.

Extended Data Fig. 1 | BRCA1–BARD1 stimulates long-range resection by WRN-DNA2-RPA. a, Molecular weight distributions of 2xMBP-tagged BRCA1 alone or in complex with BARD1 measured by mass photometry. Black asterisks (*) indicate background noise. **b**, Polyacrylamide gels of the indicated recombinant proteins stained with Coomassie Brilliant Blue. **c**, DNA endonuclease assays with MRN-pCtIP, in the absence or presence of BRCA1-BARD1. Top, a schematic of the assay. Red asterisk (*) represents the position of the radioactive label. Middle, quantitation of DNA degradation. Averages shown; error bars, SEM; n = 3. Bottom, representative assays. **d**, DNA exonuclease assays with MR, in the absence or presence of either BRCA1 or BRCA1-BARD1. Right, a schematic of the substrate. Red asterisk (*) represents the position of the radioactive label. Top left, quantitation of the different reaction intermediates. Averages shown; error bars, SEM; n = 3. Bottom, representative assays. **e**, Representative kinetic resection assays with WRN-DNA2-RPA, in the absence or presence of BRCA1-BARD1. **f**, Representative resection assays with RPA and the indicated concentrations of WRN in the absence or presence of BRCA1-BARD1 and DNA2. For this assay 0.2 nM of radioactively labeled substrate was used. **g**, 2xMBP-BRCA1-BARD1 either mock-treated or treated with PreScission protease (1:5 ratio, w:w) for 1 h at 4 °C. The polyacrylamide gel was stained with Coomassie Brilliant Blue. **h**, Representative resection assays on with WRN-DNA2-RPA, in the absence or presence of BRCA1-BARD1, either mock- or PreScission protease-treated. **i**, Polyacrylamide gels of the indicated recombinant WRN and DNA2 variants stained with Coomassie Brilliant Blue. **j**, Representative resection assays with wild type WRN or helicase-dead WRN K577M, wild type DNA2, helicase-dead DNA2 K654R or nuclease-dead DNA2 D277A, RPA, in the absence or presence of BRCA1-BARD1. ATP was omitted or substituted with non-hydrolysable ATP analogs (ATP-γ-S or AMP-PNP) as indicated. Source data are provided as Supplementary Information SI Fig. 4.

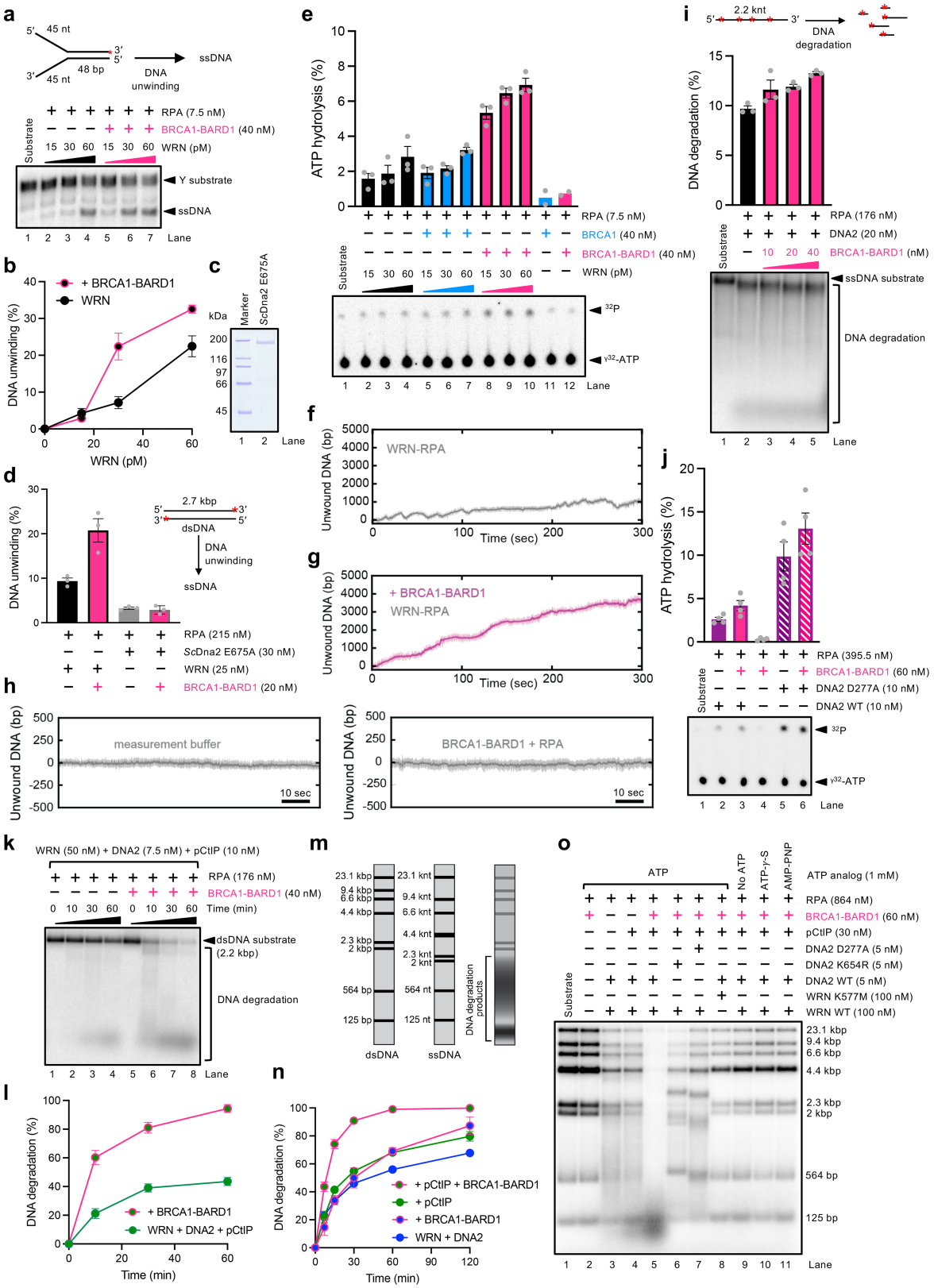

Extended Data Fig. 2 | See next page for caption.

Extended Data Fig. 2 | BRCA1-BARD1 stimulates ATP-dependent WRN helicase. a, Unwinding assays with WRN-RPA, in the absence or presence of BRCA1-BARD1. Top, a schematic of the assay. Red asterisk (*) represents the position of the radioactive label. Bottom, representative assays. **b**, Quantitation of DNA unwinding assays such as shown in a. Averages shown; error bars, SEM; n = 3. **c**, Recombinant nuclease-dead yeast Dna2 E675A used in this study. The polyacrylamide gel was stained with Coomassie Brilliant Blue. **d**, Quantitation of unwinding assays with WRN-RPA or nuclease-dead yeast Dna2 E675A and RPA, in the absence or presence of BRCA1-BARD1. Averages shown; error bars, SEM; n = 3. Top right, a schematic of the assay. Red asterisk (*) represents the position of the radioactive labels. **e**, ATPase assays with a 93 nt-long ssDNA, WRN and RPA, in the absence or presence of either BRCA1 or BRCA1-BARD1. Top, quantitation of ATP hydrolysis. Averages shown; error bars, SEM (lanes 2-10); n = 2 for BRCA1 and BRCA1-BARD1 alone controls and n = 3 for all the other samples. Bottom, representative assays. **f**, Representative trajectory of DNA unwinding events by WRN in the presence of RPA, both 25 nM. **g**, Representative trajectory of DNA unwinding events by WRN (25 nM) in the presence of BRCA1-BARD1 (40 nM) and RPA (25 nM). **h**, Representative trajectories with the reaction buffer (left) or BRCA1-BARD1 (40 nM) and RPA (25 nM) alone (right). **i**, Nuclease assays with DNA2-RPA, in the absence or presence of BRCA1-BARD1. Top, a schematic of the assay. Red asterisks (*) represent the position of the radioactive labels. Middle, quantitation of the DNA degradation products. Averages shown; error bars, SEM; n = 3. Bottom, representative assays. **j** ATPase assays in the presence of 10.3 knt-long ssDNA with wild type DNA2 or nuclease-dead DNA2 D277A and RPA, in the absence or presence of BRCA1-BARD1. Top, quantitation of ATP hydrolysis. Averages shown; error bars, SEM; n = 4. Bottom, representative assays. **k**, Representative kinetic assays with WRN-DNA2-RPA, phosphorylated CtIP (pCtIP), in the absence or presence of BRCA1-BARD1. **l**, Quantitation of DNA degradation products from assays such as shown in k. Averages shown; error bars, SEM; n = 3. **m**, A schematic of the λ DNA/HindIII-based substrate employed for the DNA end resection assays. Shown is the distribution of the DNA fragments in their double-stranded (left) or single-stranded (middle) forms. The right lane shows an example of a pattern upon partial DNA degradation. **n**, Quantitation of DNA degradation products (based on disappearance of DNA fragments of ≥4.3 kbp in length) from assays such as shown in Fig. 3a. Averages shown; error bars, SEM; n = 3. **o**, Representative resection assays with wild type WRN or helicase-dead WRN K577M, wild type DNA2, or helicase-dead DNA2 K654R or nuclease-dead DNA2 D277A, pCtIP and RPA, in the absence or presence of BRCA1-BARD1. ATP was omitted or substituted with non-hydrolysable ATP analogs (ATP-γ-S or AMP-PNP) as indicated. Source data are provided as Supplementary Information SI Fig. 5.

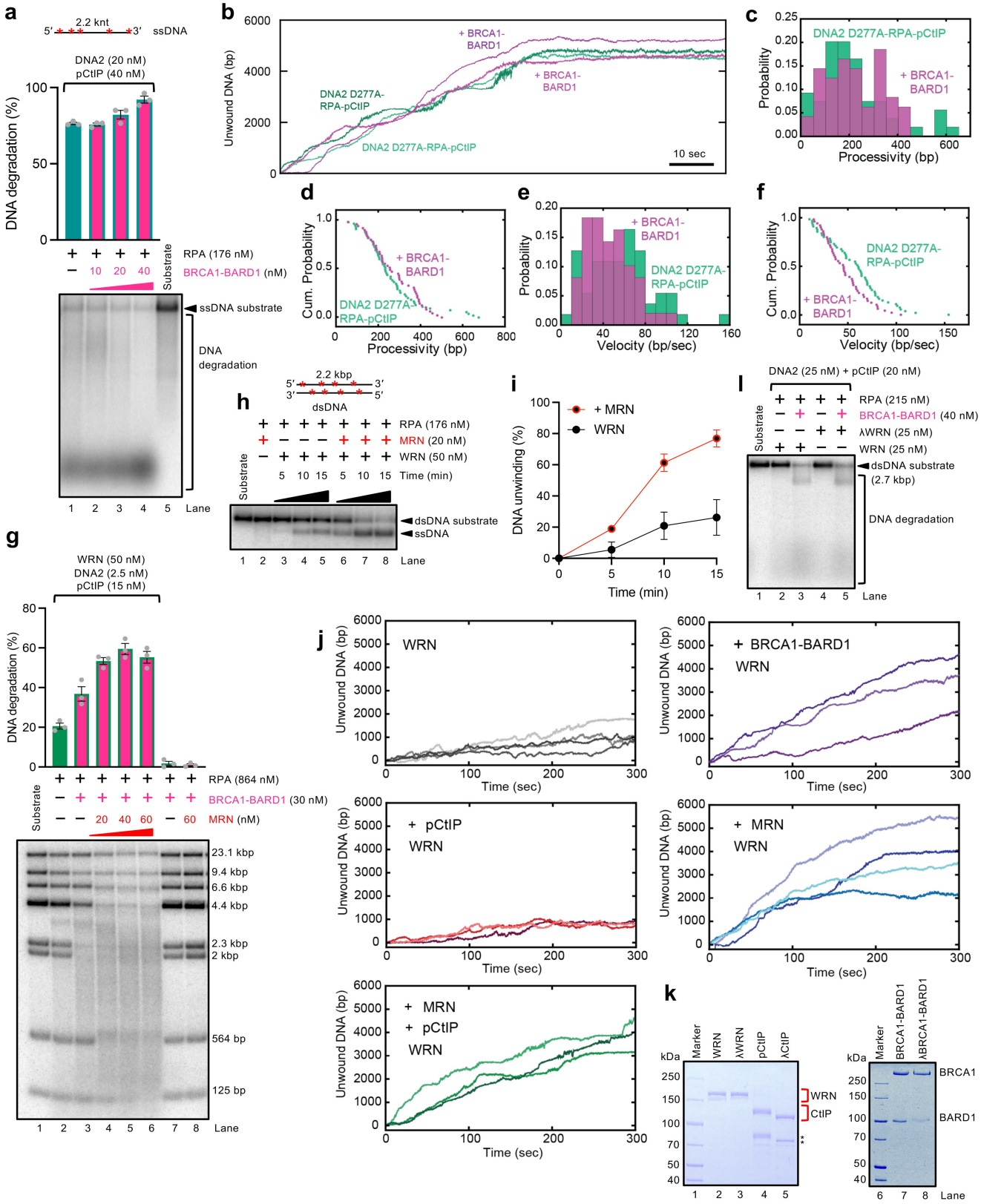

Extended Data Fig. 3 | See next page for caption.

Extended Data Fig. 3 | The BRCA1-C complex stimulates resection by WRN-DNA2-RPA. a, Nuclease assays with DNA2-pCtIP-RPA, in the absence or presence of BRCA1-BARD1. Top, a schematic of the substrate. Middle, quantitation of DNA degradation. Averages shown; error bars, SEM; n = 3. Bottom, representative assays. **b**, Representative trajectories of DNA unwinding events by nuclease-dead DNA2 D277A (10 nM) with pCtIP (10 nM) and RPA (25 nM), in the absence (green) or presence (pink) of BRCA1-BARD1 (25 nM). **c**, **d**, Processivity histogram and cumulative probability distribution (shown as survival probability) of the observed DNA unwinding events by nuclease-dead DNA2 D277A-pCtIP-RPA, in the absence (green) or presence (pink) of BRCA1-BARD1, with mean values of 264 ± 38 bp (n = 55) and 271 ± 32 bp (n = 49), respectively. Error, 2SEM. **e**, **f**, Velocity histogram and cumulative probability distribution (shown as survival probability) of the observed DNA unwinding events by nuclease-dead DNA2 D277A-pCtIP-RPA, in the absence (green) or presence (pink) of BRCA1-BARD1, with mean values of 57 ± 8 bp/sec (n = 55) and 46 ± 6 bp/sec (n = 49), respectively. Error, 2SEM. **g**, Representative resection assays with WRN-DNA2-pCtIP-RPA, BRCA1-BARD1, and the indicated concentration of MRN. Top, quantitation of DNA degradation products (based on disappearance of DNA fragments of ≥4.3 kbp in length). Averages shown; error bars, SEM; n = 3. **h**, Representative kinetic resection assays with WRN-RPA, in the absence or presence of MRN. **i**, Quantitation of DNA unwinding assays such as shown in h. Averages shown; error bars, SEM; n = 3. **j**, Representative trajectories of DNA unwinding events by WRN, in the absence or presence of the indicated proteins, all at 25 nM. **k**, Polyacrylamide gels of the indicated recombinant proteins stained with Coomassie Brilliant Blue (relevant proteins indicated with red brackets). Black asterisks (*) represent truncations of the indicated proteins (lanes 4 and 5). **l**, Representative resection assays with DNA2-pCtIP-RPA, in the presence of WRN (WRN) or de-phosphorylated WRN (λWRN), and in the absence or presence of BRCA1-BARD1. Source data are provided as Supplementary Information SI Fig. 6.

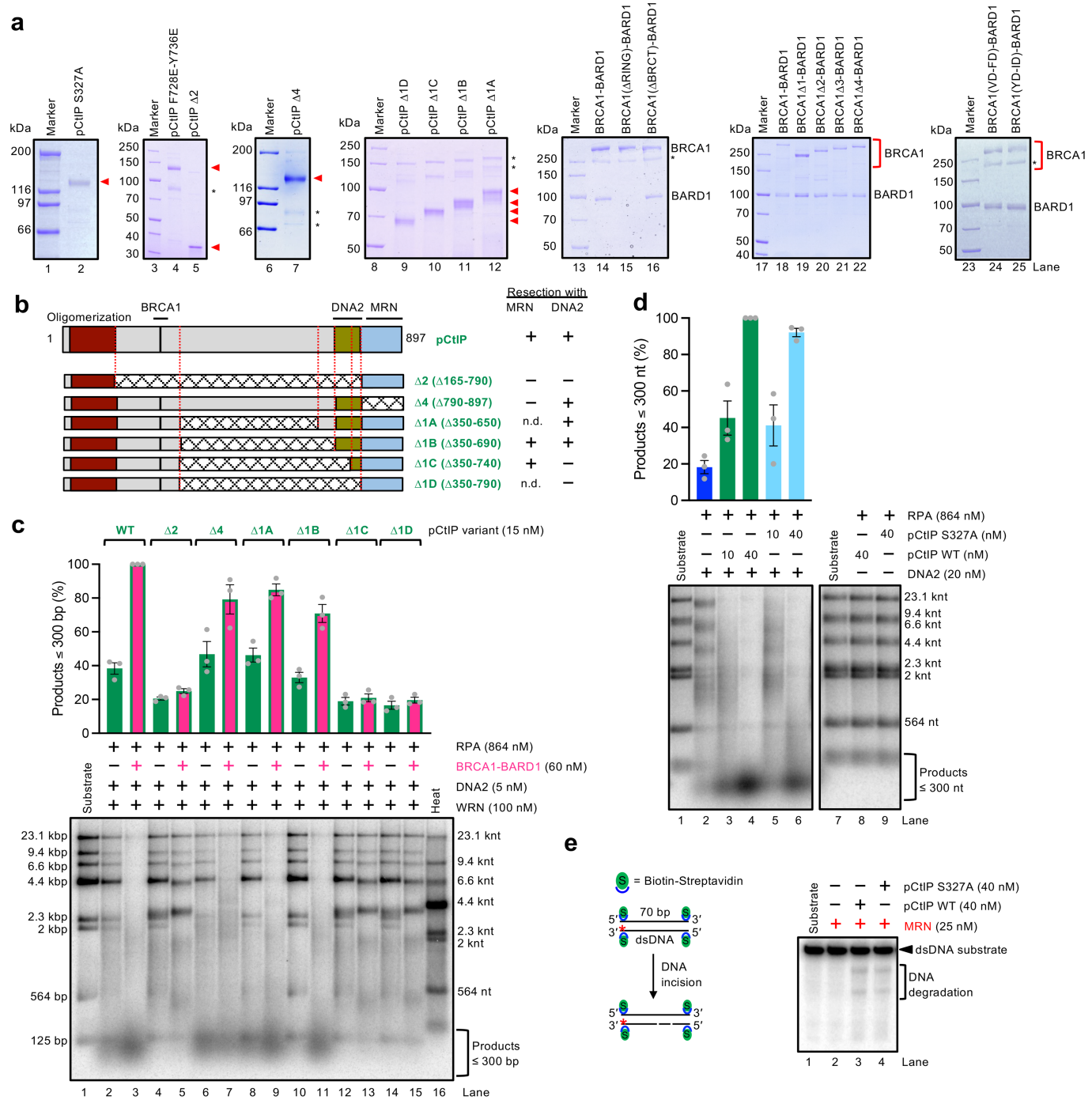

Extended Data Fig. 4 | CtIP interaction with BRCA1 and DNA2 is required for its function in the long-range DNA end resection ensemble. **a**, Polyacrylamide gels of the indicated recombinant proteins stained with Coomassie Brilliant Blue (relevant proteins indicated with red arrows or red brackets). Black asterisks (*) represent truncations of the indicated proteins (lanes 5, 7), proteins with uncleaved MBP-tag (lanes 9-12) or proteins with some spontaneous cleavage of the MBP-tag (lanes 14-16 and 25). BRCA1 VD-FD, V1035D-F1036D (lane 24). BRCA1 YD-ID, Y1127D-I1129D (lane 25). **b**, Cartoon of the primary structure of the phosphorylated CtIP (pCtIP) variants used in this study. Deleted portions of the protein are indicated with a diamond grid pattern. The capacity of each variant to stimulate MRN and/or DNA2-mediated resection, as reported from previous studies, is indicated on the right. n.d., not determined. **c**, Resection assays with WRN-DNA2-RPA, in the absence or presence of BRCA1-BARD1 and the indicated pCtIP variant (see panel b). Top, quantitation of DNA degradation products of ≤300 bp in length. Averages shown; error bars, SEM; n = 3. Bottom, representative assays. **d**, Resection assays showing the substrate degradation by DNA2-RPA, in the presence of either wild type pCtIP or pCtIP S327A variant. Top, quantitation of DNA degradation products of ≤300 bp in length. Averages shown; error bars, SEM; n = 3. Bottom, representative assays. **e**, Nuclease assays with MRN, in the presence of either wild type pCtIP or pCtIP S327A variants. Left, a schematic of the assay. Red asterisk (*) represents the position of the radioactive label. Right, representative assays. Source data are provided as Supplementary Information SI Fig. 7.

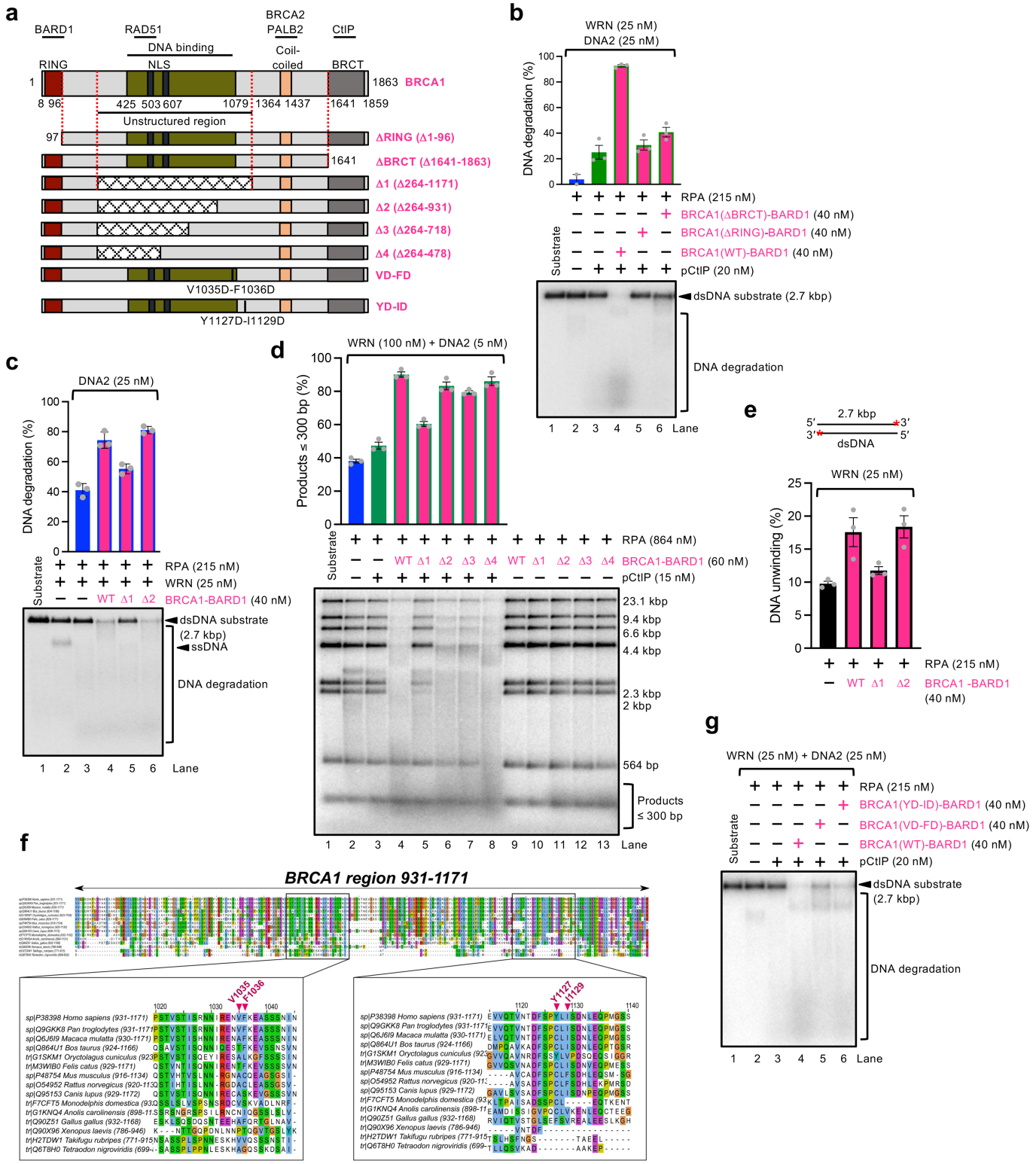

Extended Data Fig. 5 | Identification of BRCA1 regions necessary for DNA end resection. a, Cartoon of the primary structure of the BRCA1 protein including all variants used in this study. Deleted segments of the proteins are indicated with diamond grid pattern. **b**, Resection assays with WRN-DNA2-pCtIP-RPA, in the absence or presence of the indicated BRCA1 variants in complex with BARD1. Top, quantitation of DNA degradation. Averages shown; error bars, SEM; n = 3. Bottom, representative assays. **c**, Resection assays with WRN-DNA2-RPA, in the absence or presence of the indicated BRCA1 variants in complex with BARD1. Top, quantitation of DNA degradation. Averages shown; error bars, SEM; n = 3. Bottom, representative assays. **d**, Resection assays with WRN-DNA2-RPA, in absence or presence of pCtIP and the indicated BRCA1-BARD1 variants. Top, quantitation of DNA degradation products of ≤300 bp in length. Averages shown; error bars, SEM; n = 3. Bottom, representative assays. **e**, Unwinding assays with WRN-RPA, in the absence or presence of the indicated BRCA1-BARD1 variants. Averages shown; error bars, SEM; n = 3. Top, a schematic of the substrate. Red asterisk (*) represents the position of the radioactive label. **f**, Alignment of BRCA1 region 931-1171. Selected residues mutated in this study are highlighted by pink triangles. Insertions in the orthologs of human BRCA1 are not shown. **g**, Representative resection assays with WRN-DNA2-pCtIP-RPA, in the absence or presence of the indicated BRCA1 variants in complex with BARD1. Source data are provided as Supplementary Information SI Fig. 8.

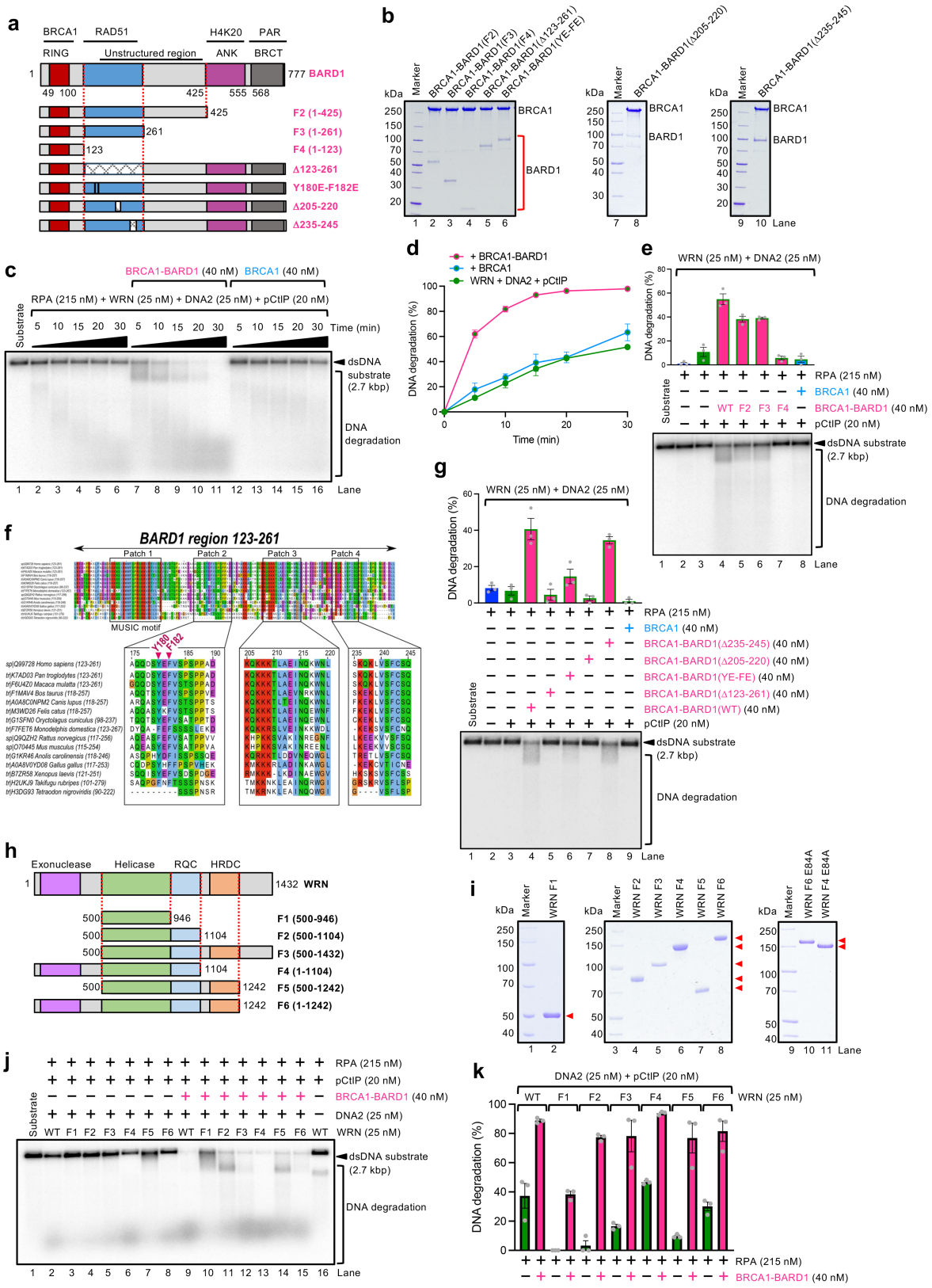

Extended Data Fig. 6 | See next page for caption.

Extended Data Fig. 6 | Identification of BARD1 and WRN regions necessary for DNA end resection. a, Cartoon of the primary structure of BARD1 and the truncated variants used in this study. **b**, Polyacrylamide gels of the indicated BARD1 variants stained with Coomassie Brilliant Blue. **c**, Representative kinetic resection assays with WRN-DNA2-pCtIP-RPA, in the absence or presence of either BRCA1-BARD1 or BRCA1. **d**, Quantitation of DNA degradation from assays such as shown in c. Averages shown; error bars, SEM; n = 3. **e**, Resection assays with WRN-DNA2-pCtIP-RPA, in the absence or presence of the indicated BARD1 variants in complex with BRCA1. Top, quantitation of DNA degradation. Averages shown; error bars, SEM; n = 3. Bottom, representative assays. **f**, Alignment of the BARD1 region 123-261. Selected patches and residues mutated in this study are highlighted. Insertions in the orthologs of human BARD1 are not shown. **g**, Resection assays with WRN-DNA2-pCtIP-RPA, in the absence or presence of the indicated BARD1 variant, expressed as BRCA1-BARD1. Top, quantitation of DNA degradation. Averages shown; error bars, SEM; n = 3. Bottom, representative assays. **h**, Cartoon of the primary structure of the WRN protein and the truncated variants used in this study. **i**, Polyacrylamide gels of the indicated recombinant proteins stained with Coomassie Brilliant Blue (relevant proteins indicated with red arrows). **j**, Representative resection assays with DNA2-pCtIP-RPA and the indicated WRN variant, in the absence or presence of BRCA1-BARD1. **k**, Quantitation of DNA degradation product from resection assays such as shown in i. Averages shown; error bars, SEM; n = 3. Source data are provided as Supplementary Information SI Fig. 8.

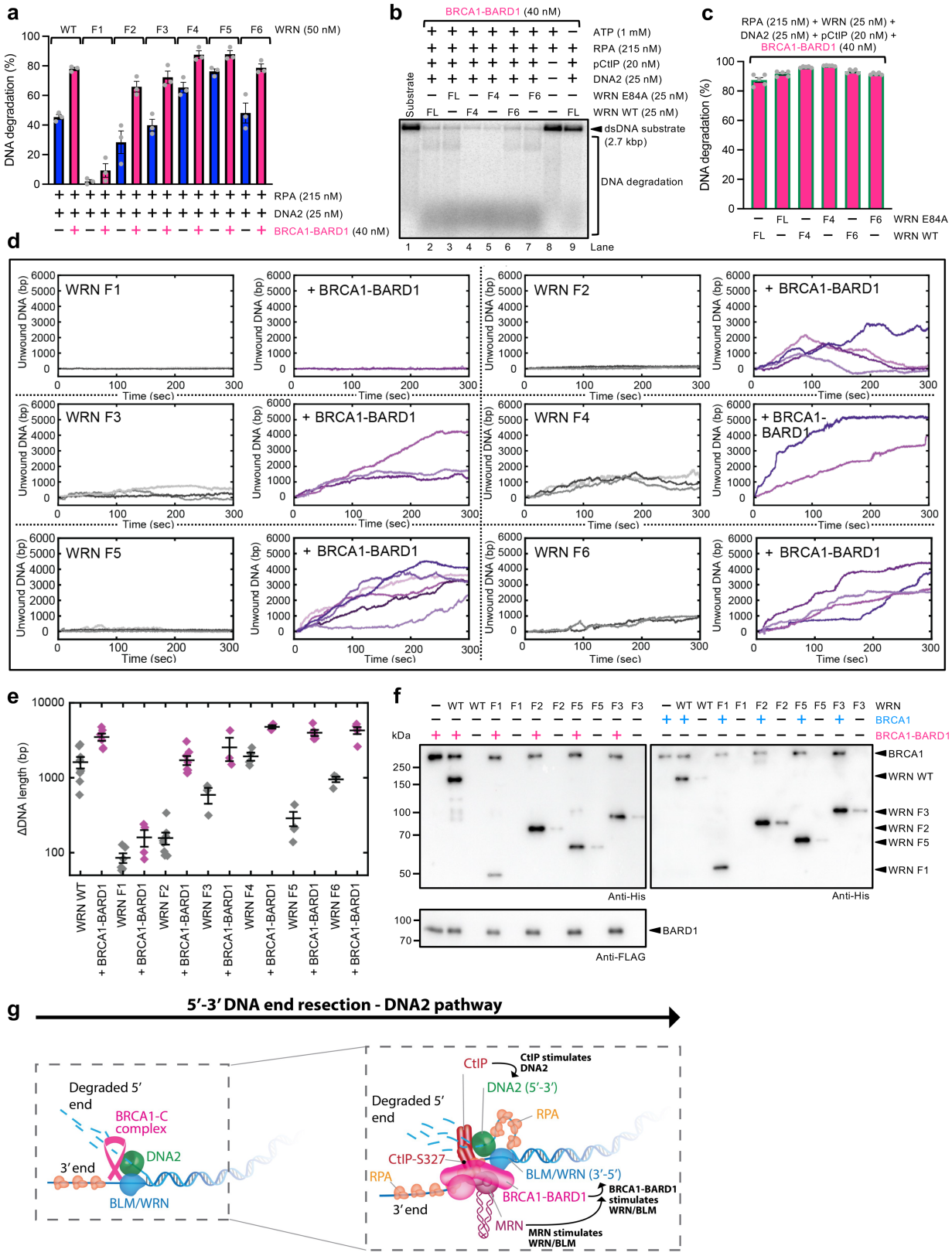

Extended Data Fig. 7 | See next page for caption.

Extended Data Fig. 7 | BRCA1 interacts with WRN through multiple contact points. a, Quantitation of DNA degradation products from resection assays with DNA2- RPA, in the absence or presence of BRCA1-BARD1 and the indicated WRN variant. Averages shown; error bars, SEM; n = 3. **b**, Representative resection assays with DNA2-pCtIP-RPA, the indicated WRN variant and BRCA1-BARD1. FL, full-length WRN protein. **c**, Quantitation of DNA degradation from assays such as shown in b. Averages shown; error bars, SEM; n = 5. **d**, Representative trajectories of DNA unwinding events by the indicated WRN variant, in the absence or presence of BRCA1-BARD1, all at 25 nM. FL, full-length WRN protein. **e**, ΔDNA-length analysis of the indicated WRN variants, in the absence or presence of BRCA1-BARD1, at 25 nM. Averages shown; error bars, SEM; n = 8 (for WRN WT, WRN F2, WRN F2 + BRCA1-BARD1), n = 6 (for WRN WT + BRCA1-BARD1, WRN F1), n = 5 (for WRN F5, WRN F5 + BRCA1-BARD1, WRN F6 + BRCA1-BARD1), n = 2 (for WRN F1 + BRCA1-BARD1, WRN F4, WRN F4 + BRCA1-BARD1, WRN F6), n = 3 (WRN F3, WRN F3 + BRCA1-BARD1). **f**, Representative protein interaction assays. **g**, A model of DNA2-dependent DNA end resection pathway and its stimulation by the BRCA1-C complex. Source data are provided as Supplementary Information SI Fig. 9.

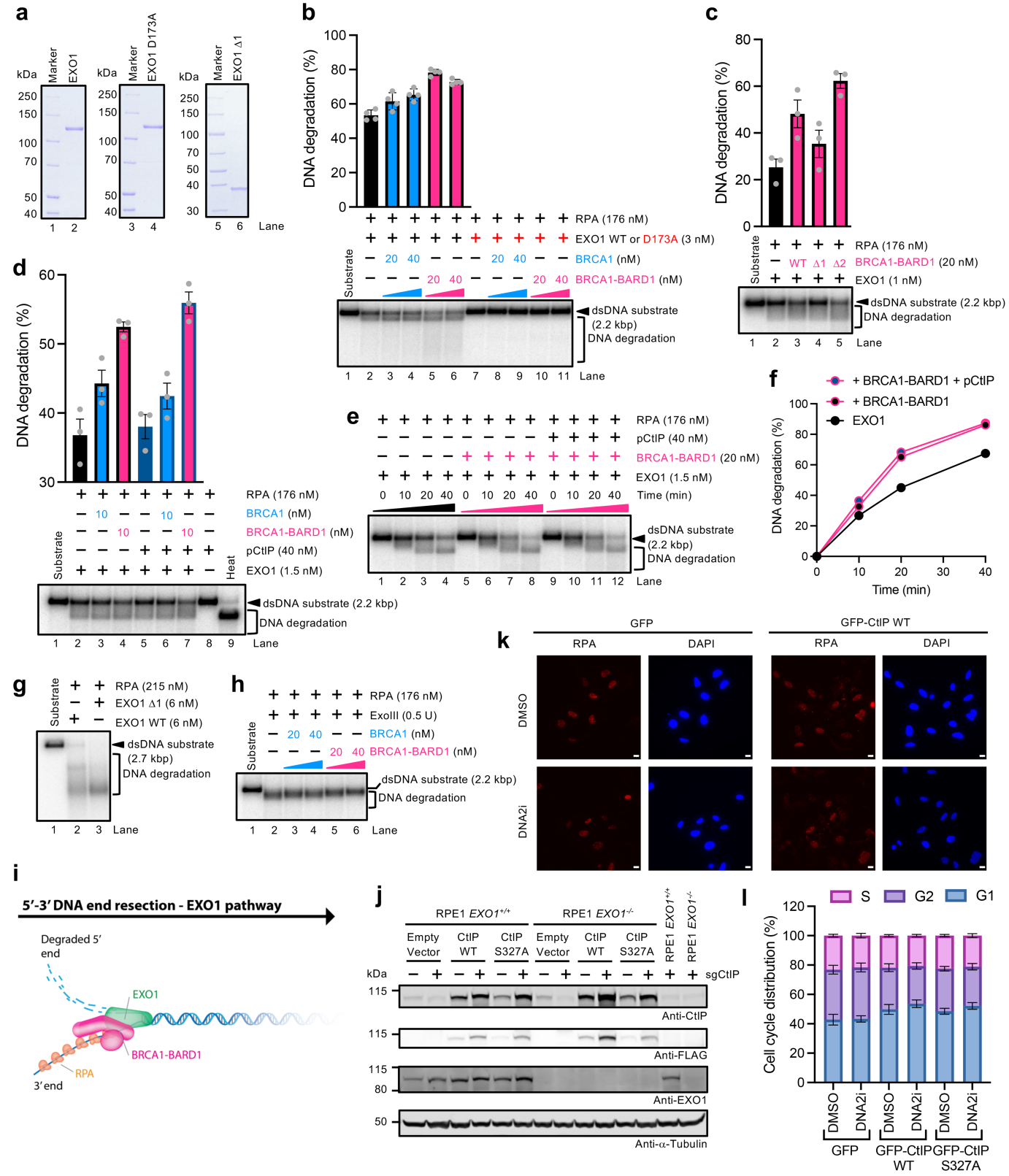

Extended Data Fig. 8 | See next page for caption.

Extended Data Fig. 8 | Stimulation of EXO1-dependent long-range DNA end resection by BRCA1-BARD1. a, Polyacrylamide gels of the indicated recombinant EXO1 variants stained with Coomassie Brilliant Blue. **b**, Resection assays with the indicated EXO1 variant and RPA, in the absence or presence of either BRCA1 or BRCA1-BARD1. Top, quantitation of DNA degradation. Averages shown; error bars, SEM; n = 4. Bottom, representative assays. **c**, Resection assays with EXO1, in the absence or presence of the indicated BRCA1-BARD1 variant. Top, quantitation of DNA degradation. Averages shown; error bars, SEM; n = 3. Bottom, representative assays. **d**, Resection assays with EXO1 and RPA, in the absence or presence of either BRCA1 or BRCA1-BARD1 and pCtIP. Top, quantitation of DNA degradation. Averages shown; error bars, SEM; n = 3. Bottom, representative assays. **e**, Representative kinetic resection assays with a randomly labeled 2.2 kbp-long dsDNA, EXO1 and RPA, in the absence or presence of BRCA1-BARD1 and pCtIP. **f**, Quantitation of DNA resection assays such as shown in e. Averages shown; error bars, SEM; n = 3. **g**, Representative assays with the indicated EXO1 variant and RPA. **h**, Representative resection assays with *E. coli* ExoIII and RPA, in the absence or presence of either BRCA1 or BRCA1-BARD1. **i**, A model of EXO1-dependent DNA end resection pathway and the involvement of BRCA1-BARD1. **j**, Western Blot analysis showing expression of lentivirally transduced FLAG-tagged CtIP WT or S327A in RPE1 *EXO1*$^{+/+}$ or *EXO1*$^{-/-}$ cells. **k**, Representative microscopy images of indicated U2OS-derived cell lines untreated (DMSO) or treated (DNA2i) with the DNA2 inhibitor C5, stained for RPA (red) or DAPI (blue). Scale bar, 10 µm. **l**, Quantitation of the cell cycle distribution of the indicated cell lines untreated (DMSO) or treated (DNA2i) with the DNA2 inhibitor C5. Source data are provided as Supplementary Information SI Figs. 9 and 10.

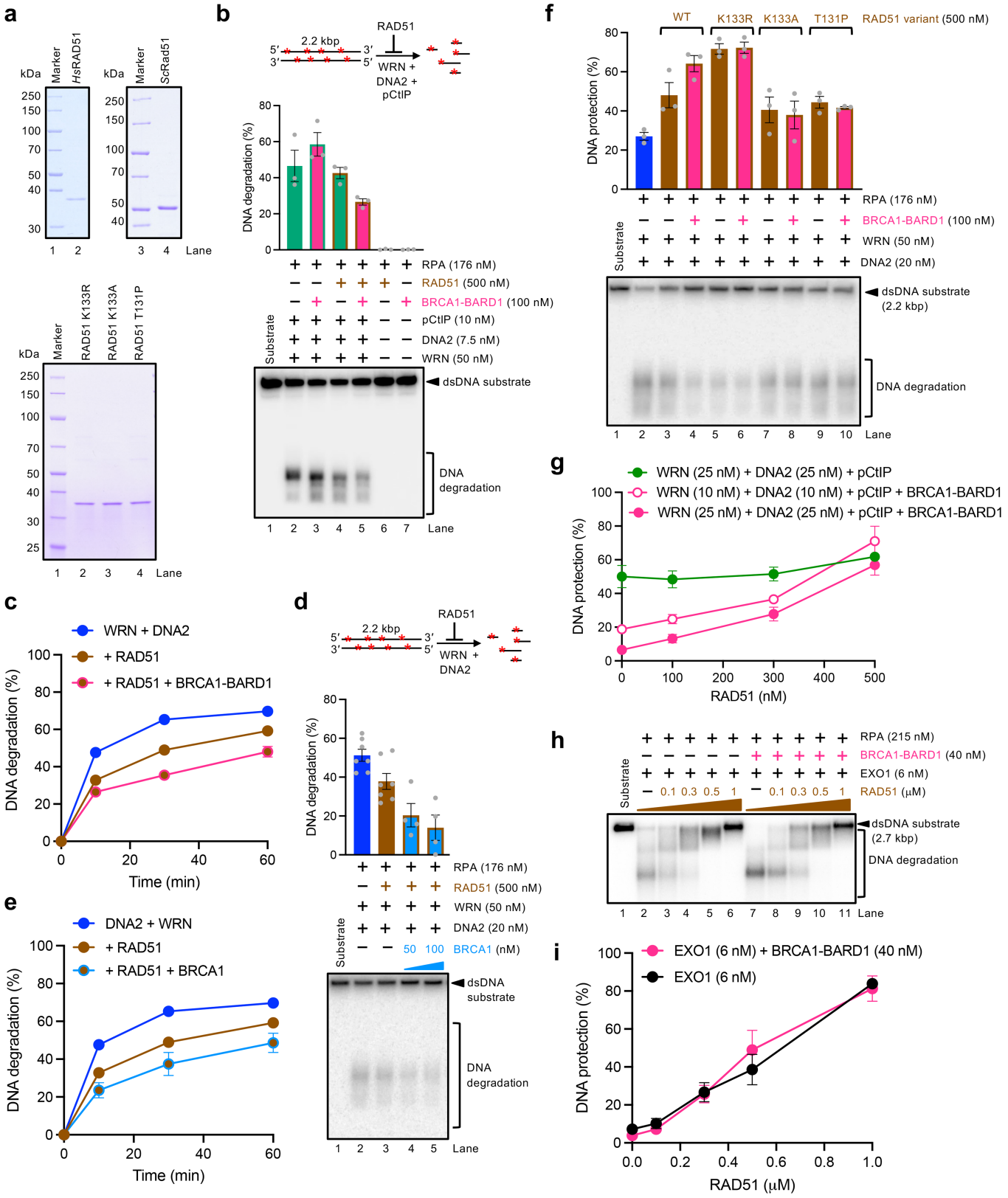

Extended Data Fig. 9 | See next page for caption.

Extended Data Fig. 9 | DNA protection by RAD51-BRCA1-BARD1 ensemble. **a**, Polyacrylamide gels of the indicated recombinant RAD51 variants stained with Coomassie Brilliant Blue. **b**, DNA protection assays with WRN-DNA2-pCtIP-RPA, in the absence or presence of BRCA1-BARD1 and RAD51, performed at 100 mM NaCl. Top, a schematic of the assay. Red asterisks (*) represent the position of the radioactive labels. Middle, quantitation of DNA degradation. Averages shown; error bars, SEM; n = 3. Bottom, representative assays. **c**, Quantitation of kinetic protection assays with WRN-DNA2-RPA, in the absence or presence of BRCA1-BARD1 and RAD51, performed at 100 mM NaCl. Averages shown; error bars, SEM; n = 2 (for DNA2-WRN), n = 7 (in the absence of BRCA1-BARD1) and n = 4 (in the presence of BRCA1). **d**, Protection assays with WRN-DNA2-RPA, in the absence or presence of BRCA1 and RAD51, performed at 100 mM NaCl. Top, a schematic of the assay. Red asterisks (*) represent the position of the radioactive labels. Middle, quantitation of DNA degradation. Averages shown; error bars, SEM; n = 7 (in the absence of BRCA1) and n = 4 (in the presence of BRCA1). Bottom, representative assays. **e**, Quantitation of kinetic protection assays with WRN-DNA2-RPA, in the absence or presence of BRCA1 and RAD51, performed at 100 mM NaCl. Quantitation of DNA degradation by WRN-DNA2, in the absence or presence of RAD51, such as shown in b is included as a reference. Averages shown; error bars, SEM; n = 2 (for DNA2-WRN), n = 7 (in the absence of BRCA1-BARD1) and n = 4 (in the presence of BRCA1). **f**, Protection assays with WRN-DNA2-RPA, in the absence or presence of BRCA1-BARD1 and the indicated RAD51 variant, performed at 100 mM NaCl. KR, K133R, defective in ATP hydrolysis; KA, K133A, defective in ATP binding; TP, T131P, impaired in DNA binding. Top, quantitation of DNA protection. Averages shown; error bars, SEM; n = 3. Bottom, representative assays. **g**, Quantitation of assays such as shown in Fig. 6b. Averages shown; error bars, SEM; n = 3. The quantitation was not normalized. Representative assays with WRN (10 nM) and DNA2 (10 nM), in presence of pCtIP and BRCA1-BARD1, not shown. **h**, Representative protection assays with EXO1-RPA, in the absence or presence of BRCA1-BARD1 and increasing concentration of RAD51. **i**, Quantitation of assays such as shown in h. Averages shown; error bars, SEM; n = 3. The quantitation was not normalized. Source data are provided as Supplementary Information SI Fig. 11.

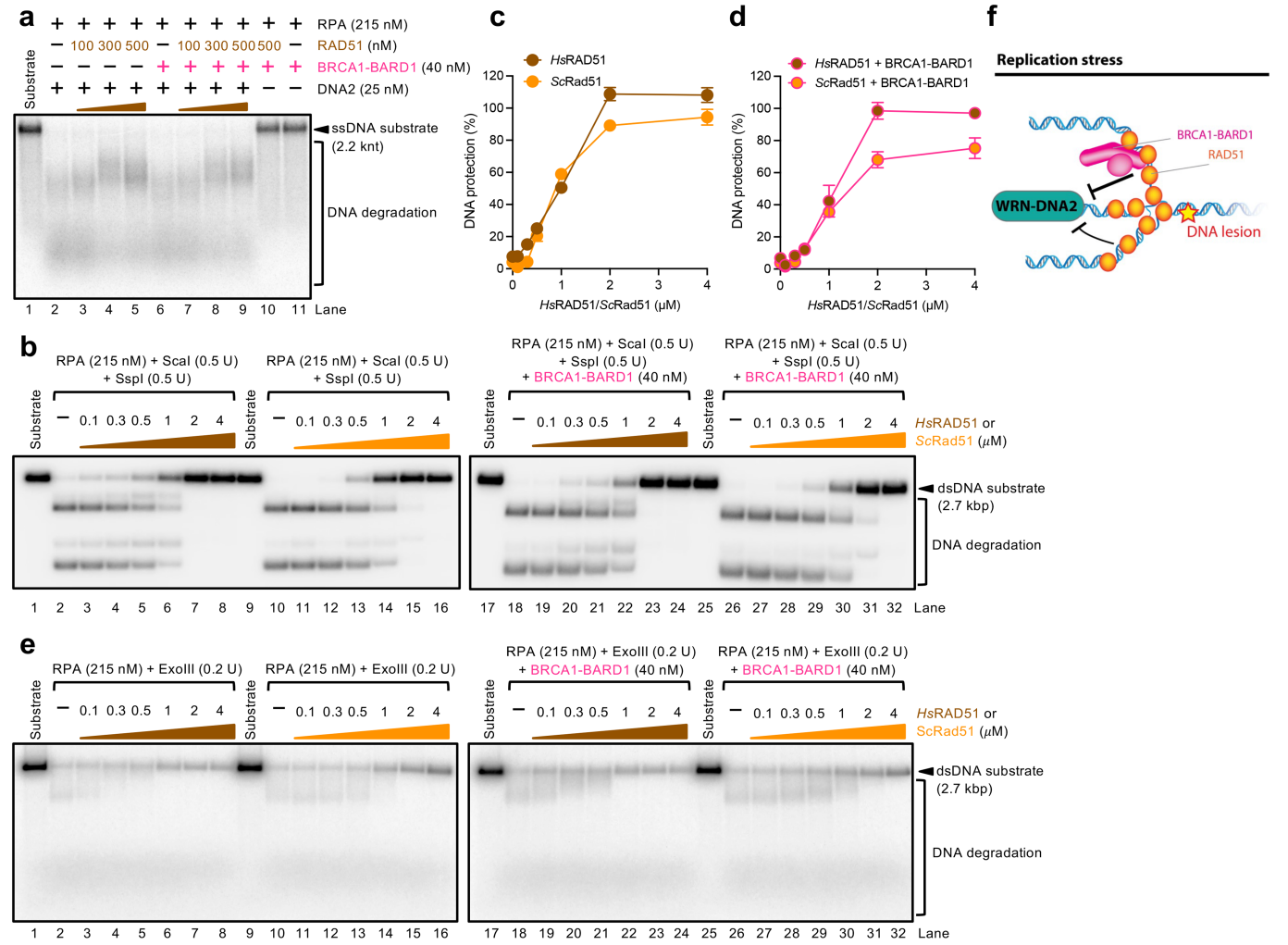

Extended Data Fig. 10 | BRCA1-BARD1 does not affect DNA degradation by non-cognate nucleases. a, Representative protection assays with DNA2-RPA, in the absence or presence of BRCA1-BARD1 and increasing concentration of RAD51. **b**, Representative protection assays with the endonucleases ScaI and SspI, with RPA and increasing concentration of human RAD51 (*Hs*RAD51) or yeast Rad51 (*Sc*Rad51) in the absence or presence of BRCA1-BARD1 **c**, Quantitation of assays such as shown in b (left). Averages shown; error bars, SEM; n = 3. **d**, Quantitation of assays such as shown in b (right). Averages shown; error bars, SEM; n = 3. **e**, Representative protection assays with *E. coli* ExoIII, with RPA and increasing concentrations of human RAD51 (*Hs*RAD51) or yeast Rad51 (*Sc*Rad51) in the absence or presence of BRCA1-BARD1. **f**, A model for DNA protection function of BRCA1-BARD1 in the presence of RAD51 upon replication stress. RAD51 inhibits DNA degradation by nucleases in an unspecific manner via its binding to dsDNA. Additionally, as shown here, RAD51, together with BRCA1-BARD1, inhibits specifically DNA2-dependent long-range resection. Source data are provided as Supplementary Information SI Fig. 11.

nature portfolio

Corresponding author(s): Petr Cejka

Last updated by author(s): Jul 18, 2024

Reporting Summary

Nature Portfolio wishes to improve the reproducibility of the work that we publish. This form provides structure for consistency and transparency in reporting. For further information on Nature Portfolio policies, see our Editorial Policies and the Editorial Policy Checklist.

Statistics

For all statistical analyses, confirm that the following items are present in the figure legend, table legend, main text, or Methods section.

n/a	Confirmed
☐	☒ The exact sample size (*n*) for each experimental group/condition, given as a discrete number and unit of measurement
☐	☒ A statement on whether measurements were taken from distinct samples or whether the same sample was measured repeatedly
☐	☒ The statistical test(s) used AND whether they are one- or two-sided *Only common tests should be described solely by name; describe more complex techniques in the Methods section.*
☒	☐ A description of all covariates tested
☒	☐ A description of any assumptions or corrections, such as tests of normality and adjustment for multiple comparisons
☐	☒ A full description of the statistical parameters including central tendency (e.g. means) or other basic estimates (e.g. regression coefficient) AND variation (e.g. standard deviation) or associated estimates of uncertainty (e.g. confidence intervals)
☐	☒ For null hypothesis testing, the test statistic (e.g. *F*, *t*, *r*) with confidence intervals, effect sizes, degrees of freedom and *P* value noted *Give P values as exact values whenever suitable.*
☒	☐ For Bayesian analysis, information on the choice of priors and Markov chain Monte Carlo settings
☒	☐ For hierarchical and complex designs, identification of the appropriate level for tests and full reporting of outcomes
☒	☐ Estimates of effect sizes (e.g. Cohen's *d*, Pearson's *r*), indicating how they were calculated

Our web collection on statistics for biologists contains articles on many of the points above.

Software and code

Policy information about availability of computer code

Data collection	We used commercial software, available as a package with the respective instrument, for data collection. This includes Typhoon FLA 9500 Phosphor Imager (GE Healthcare, Version 3.0.0.2), Fusion FX7 capture software (Vilber Imaging, Version FX7 Edge 18.12 -SN), AcquireMP (Refeyn Ltd, Version AcquireMP 2023 R1.1), Photo scanner operated with Epson Scan v3.9.4.0 US software and CanoScan 9000F Mark II scanner operated with ImageCapture v6.6(525) software. Magnetic tweezers were operated using a self-developed code in Labview (2016, National Instruments).
Data analysis	Only commercial or publicly available software was used for data analysis. This includes ImageJ2 (NIH, Version 2.9.0/1.53t) for the analysis of gel data; graphs and numerical data (including statistics/error bars) was analyzed and plotted by Prism10 (GraphPad, Version 10.0.3). Mass photometry measurements were analyzed using DiscoverMP software (Refeyn Ltd, Version v2023 R1.2). Single-molecules magnetic tweezer measurements were analyzed using custom written Matlab Software (Matlab R2016a academic license) for Helicase Analysis previously described in Seidel, R., Kasaciunaite, K., & Göse, M. (2021) (1.0.0) [Data set]. Zenodo. https://doi.org/10.5281/zenodo.5524562. Data analysis as well as plotting of magnetic tweezers data was carried out in Origin 2019. Multiple sequence alignment was performed with MAFFT multiple sequence alignment software version 7 and visualized with Jalview Version 2. RPA foci immunofluorescence was analyzed using a Leica DM6000B Fluorescence microscope (AF6000). Cell cycle distribution data were analyzed using a LSRFortessaTM Cell Analyzer (BD) Flow Cytometer and ModFit LT 5.0 software (Verity Soft-ware House Inc).

For manuscripts utilizing custom algorithms or software that are central to the research but not yet described in published literature, software must be made available to editors and reviewers. We strongly encourage code deposition in a community repository (e.g. GitHub). See the Nature Portfolio guidelines for submitting code & software for further information.

Data

Policy information about availability of data

All manuscripts must include a data availability statement. This statement should provide the following information, where applicable:

- Accession codes, unique identifiers, or web links for publicly available datasets
- A description of any restrictions on data availability
- For clinical datasets or third party data, please ensure that the statement adheres to our policy

All relevant data generated or analyzed during this study are included in this published arti-cle and its supplementary information file. Movies underlying mass photometry analysis and single-molecule source data are uploaded to Dryad (https://doi.org/10.5061/dryad.gf1vhhmxc). The link will be publicly accessible upon evaluation by the Dryad team. in the meantime, please use the following temporary link: https://datadryad.org/stash/share/obUd9u9dg5tI2zT1m6uU40kXNyRidi2BCdh6iFfKCgA
Source data are provided with this paper including uncropped images of gels and blots. This paper does not report any original code.

Research involving human participants, their data, or biological material

Policy information about studies with human participants or human data. See also policy information about sex, gender (identity/presentation), and sexual orientation and race, ethnicity and racism.

Reporting on sex and gender	N/A
Reporting on race, ethnicity, or other socially relevant groupings	N/A
Population characteristics	N/A
Recruitment	N/A
Ethics oversight	N/A

Note that full information on the approval of the study protocol must also be provided in the manuscript.

Field-specific reporting

Please select the one below that is the best fit for your research. If you are not sure, read the appropriate sections before making your selection.

☒ Life sciences ☐ Behavioural & social sciences ☐ Ecological, evolutionary & environmental sciences

For a reference copy of the document with all sections, see nature.com/documents/nr-reporting-summary-flat.pdf

Life sciences study design

All studies must disclose on these points even when the disclosure is negative.

Sample size	Sample size (or number of repeats) was chosen based on what is common in the field, and what was practical to do. A minimum of three independent replicates was performed for each experiment in order to add statistical analysis, when required, as stated in the Methods section of the manuscript.
Data exclusions	In general, no data were excluded unless there was a valid reason to do so, e.g. experiments with failed positive controls indicating technical problems, or when loading control indicated unequal loading that invalidated the analysis or other technical issues (broken gels, collapsed wells in gels etc.).
Replication	Most biochemical experiments were performed at least three times, as defined in Figure legends. Oftentimes, even within a single experiment, multiple enzyme concentrations were analyzed, or samples were compared at multiple time points. This also contributes to the robustness of the data. Experiments that could not be reproduced are not presented in this study.
Randomization	Randomization is not relevant to the experiments performed in this study. This study is not sensitive to any biased analysis.
Blinding	Blinding is not relevant to the experiments performed in this study, as measurements were objectively quantified by dedicated software or simply visually presented. Furthermore, the loading order or samples on gels prevented blinding.

Reporting for specific materials, systems and methods

We require information from authors about some types of materials, experimental systems and methods used in many studies. Here, indicate whether each material, system or method listed is relevant to your study. If you are not sure if a list item applies to your research, read the appropriate section before selecting a response.

Materials & experimental systems

n/a	Involved in the study
☐	☒ Antibodies
☐	☒ Eukaryotic cell lines
☒	☐ Palaeontology and archaeology
☒	☐ Animals and other organisms
☒	☐ Clinical data
☒	☐ Dual use research of concern
☒	☐ Plants

Methods

n/a	Involved in the study
☒	☐ ChIP-seq
☐	☒ Flow cytometry
☒	☐ MRI-based neuroimaging

Antibodies

Antibodies used

We used the following antibodies for Western blotting: mouse anti-BRCA1 (D9) antibody (Santa Cruz Biotechnology, sc-6954, 1:1,000, mouse monoclonal, Lot #L2618), mouse anti-WRN (8H3) (Cell Signaling, 4666S, 1 microgram used for immobilization in protein interaction assays), rabbit anti-His antibody (Invitrogen PA1-983B, 1:1,000, rabbit polyclonal), mouse anti-FLAG M2 antibody (Sigma, F3165, 1:1,000, mouse monoclonal, Lot #SLCC4005), goat anti-mouse-HRP conjugated (Southern Biotech, 1031-05, 1:5,000, Lot #H0021-MA82E, goat polyclonal), donkey anti-rabbit-HRP conjugated (Cytiva, NA934V, 1:5,000, donkey polyclonal), mouse anti-CtIP clone 14-1 (Millipore, MABE1060, 1:2,000, mouse monoclonal), mouse anti-FLAG M2 (Sigma, F1804-200UG, 1:2,000, mouse monoclonal), rabbit anti-EXO1 (Abcam, ab95068, 1:1,000, rabbit polyclonal), mouse anti-alpha-Tubulin DM1A (Sigma, T6199, 1:5,000, mouse monoclonal), donkey anti-rabbit IgG-HRP (Thermo Scientific, 31458, 1:5,000, donkey polyclonal), goat anti-mouse IgG-HRP (Thermo Scientific, 31432, 1:5,000, goat polyclonal), mouse anti-RPA2 (9H8) antibody (Abcam, ab2175, 1:500, mouse monoclonal), goat anti-mouse Alexa Fluor 594 (Invitrogen, A11032, 1:500, goat polyclonal), goat anti-rabbit Alexa Fluor 488 (Invitrogen, A11034, 1:500, goat polyclonal).

Validation

The specificity of the rabbit anti-His (Invitrogen PA1-983B, 1:1,000, rabbit polyclonal) antibody is indicated in Figure 2i using untagged BRCA1- BARD1 protein in absence or presence of WRN, as well as WRN protein alone. The specificity of the mouse anti-BRCA1 (Santa Cruz Biotechnology, sc-6954) and mouse anti-FLAG antibody (Sigma, F3165) are indicated in Figure 5e using EXO1-FLAG sample in absence or presence of BRCA1-BARD1 protein. The specificity of the mouse anti-CtIP clone 14-1 (Millipore, MABE1060, 1:2,000, mouse monoclonal), mouse anti-FLAG (Sigma, F1804-200UG, 1:2,000, mouse monoclonal), rabbit anti-EXO1 (Abcam, ab95068, 1:1,000, rabbit polyclonal) are indicated in Extended Data Fig. 8j. Mouse anti-WRN (8H3) (Cell Signaling, 4666S, 1 microgram used for immobilization in protein interaction assays) was validated for the following applications: Simple Western and Western Blot as stated on the manufacturer's website. Mouse anti-alpha-Tubulin DM1A (Sigma, T6199, 1:5,000, mouse monoclonal) has been used in immunocytofluorescence and western blot analysis as stated on the manufacturer's website. Mouse anti-RPA2 (9H8) antibody (Abcam, ab2175, 1:500, mouse monoclonal) is suitable for IHC-P, Flow Cyt, WB and reacts with human samples as stated upon enhance validation process on the manufacturer's website.

Eukaryotic cell lines

Policy information about cell lines and Sex and Gender in Research

Cell line source(s)

The HEK 293T cell line was originally purchased from ATCC. RPE1-hTERT cells were purchased from ATCC. GFP, GFP-CtIP WT or GFP-CtIP S327A U2OS cell lines used are derived from U2OS, that was originally bought from ATCG.

Authentication

The HEK 293T cell line was checked by morphology. Genetic editing of RPE1-hTERT cell lines was confirmed by PCR-based Sanger sequencing of edited locus. U2OS cells were last authenticated in June 2024 by the GenePrint® 10 System (Promega, Madison, WI, USA) using STR profiling, and data were analyzed using genemapper® id-x v1.2 software (Applied Biosystems, Waltham, MA, USA) at the genomic core facility of the Instituto de Investigaciones Biomedicas Sols-Morreale.

Mycoplasma contamination

We routinely test for mycoplasm for all cell lines. All the experiments performed here were using mycoplas-free cell lines

Commonly misidentified lines
(See ICLAC register)

None

Plants

Seed stocks	*Report on the source of all seed stocks or other plant material used. If applicable, state the seed stock centre and catalogue number. If plant specimens were collected from the field, describe the collection location, date and sampling procedures.*
Novel plant genotypes	*Describe the methods by which all novel plant genotypes were produced. This includes those generated by transgenic approaches, gene editing, chemical/radiation-based mutagenesis and hybridization. For transgenic lines, describe the transformation method, the number of independent lines analyzed and the generation upon which experiments were performed. For gene-edited lines, describe the editor used, the endogenous sequence targeted for editing, the targeting guide RNA sequence (if applicable) and how the editor was applied.*
Authentication	*Describe any authentication procedures for each seed stock used or novel genotype generated. Describe any experiments used to assess the effect of a mutation and, where applicable, how potential secondary effects (e.g. second site T-DNA insertions, mosiacism, off-target gene editing) were examined.*

Flow Cytometry

Plots

Confirm that:

☒ The axis labels state the marker and fluorochrome used (e.g. CD4-FITC).

☒ The axis scales are clearly visible. Include numbers along axes only for bottom left plot of group (a 'group' is an analysis of identical markers).

☒ All plots are contour plots with outliers or pseudocolor plots.

☒ A numerical value for number of cells or percentage (with statistics) is provided.

Methodology

Sample preparation	Cells were fixed with cold 70% ethanol for at least 2 hours, incubated with 250 g/ml RNase A (Sigma Aldrich) and 10 g/ml propidium iodide (Sigma Aldrich) at 37 °C for 30 min.
Instrument	Samples were analysed with a LSRFortessaTM Cell Analyzer (BD) Flow Cytometer.
Software	Cell cycle distribution data were further analysed using ModFit LT 5.0 software (Verity Software House Inc).
Cell population abundance	N/A Sorting was not performed.
Gating strategy	A. Forward vs side scatter plot showing gate P1 around cells and excluding cell debris. B. Propidium iodide in the FL2 width vs propidium iodide in the FL2 area showing events from P1, with single cells gated within P2. C. Cell cycle analysis calculated G1, S and G2M phase from a FL2-A histogram showing events from P1+P2.

☒ Tick this box to confirm that a figure exemplifying the gating strategy is provided in the Supplementary Information.